

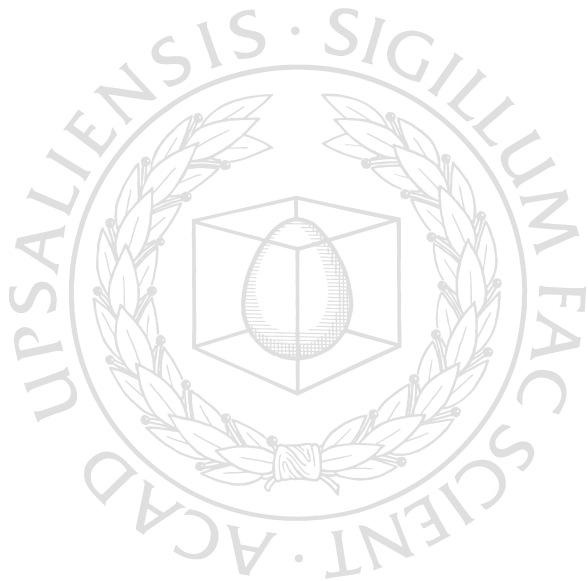


UPPSALA
UNIVERSITET

*Digital Comprehensive Summaries of Uppsala Dissertations
from the Faculty of Science and Technology 1043*

Relating the Bulk and Interface Structure of Hyaluronan to Physical Properties of Future Biomaterials

IDA BERTS



ACTA
UNIVERSITATIS
UPSALIENSIS
UPPSALA
2013

ISSN 1651-6214
ISBN 978-91-554-8669-3
urn:nbn:se:uu:diva-198357

Dissertation presented at Uppsala University to be publicly examined in Högssalen, Ångströmlaboratoriet, Lägerhyddsvägen 1, Uppsala, Wednesday, June 5, 2013 at 09:00 for the degree of Doctor of Philosophy. The examination will be conducted in English.

Abstract

Berts, I. 2013. Relating the Bulk and Interface Structure of Hyaluronan to Physical Properties of Future Biomaterials. Acta Universitatis Upsaliensis. *Digital Comprehensive Summaries of Uppsala Dissertations from the Faculty of Science and Technology* 1043. 66 pp. Uppsala. ISBN 978-91-554-8669-3.

This dissertation describes a structural investigation of hyaluronan (HA) with neutron scattering techniques. HA is a natural biopolymer and one of the major components of the extracellular matrix, synovial fluid, and vitreous humor. It is used in several biomedical applications like tissue engineering, drug delivery, and treatment of osteoarthritis. Although HA is extensively studied, very little is known about its three-dimensional conformation and how it interacts with ions and other molecules. The study aims to understand the bulk structure of a cross-linked HA hydrogel, as well as the conformational arrangement of HA at solid-liquid interfaces. In addition, the structural changes of HA are investigated by simulation of physiological environments, such as changes in ions, interactions with nanoparticles, and proteins etc. Small-angle neutron scattering and neutron reflectivity are the two main techniques applied to investigate the nanostructure of hyaluronan in its original, hydrated state.

The present study on hydrogels shows that they possess inhomogeneous structures best described with two correlation lengths, one of the order of a few nanometers and the other in the order of few hundred nanometers. These gels are made up of dense polymer-rich clusters linked to each other. The polymer concentration and mixing governs the connectivity between these clusters, which in turn determines the viscoelastic properties of the gels. Surface-tethered HA at a solid-liquid interface is best described with a smooth varying density profile. The shape of this profile depends on the immobilization chemistry, the deposition protocol, and the ionic interactions. HA could be suitably modified to enhance adherence to metal surfaces, as well as incorporation of proteins like growth factors with tunable release properties. This could be exploited for surface coating of implants with bioactive molecules. The knowledge gained from this work would significantly help to develop future biomaterials and surface coatings of implants and biomedical devices.

Keywords: hyaluronan, structure, bulk, interface, small-angle neutron scattering, neutron reflection, hydrogel, grafting, nanoparticles, protein interactions

Ida Berts, Uppsala University, Department of Chemistry - Ångström, Box 523, SE-751 20 Uppsala, Sweden.

© Ida Berts 2013

ISSN 1651-6214

ISBN 978-91-554-8669-3

urn:nbn:se:uu:diva-198357 (<http://urn.kb.se/resolve?urn=urn:nbn:se:uu:diva-198357>)

诗书继世古
忠厚传家久

Till mormor & morfar

List of Papers

This thesis is based on the following papers, which are referred to in the text by their Roman numerals.

- I Structure of polymer and particle aggregates in hydrogel composites**
Berts, I.; Gerelli, Y.; Hilborn, J.; Rennie, A. R.
Journal of Polymer Science Part B: Polymer Physics **2013**, 51, (6), 421-429

- II Tuning the density profile of surface-grafted hyaluronan and the effect of counter-ions**
Berts, I.; Fragneto, G.; Hilborn, J.; Rennie, A. R.
European physical Journal E: Soft Matter and Biological Physics **2013**, Topical issue Neutron Biological Physics, *In press*

- III Adsorption and co-adsorption of human serum albumin and myoglobin with hyaluronan on different substrates**
Berts, I.; Fragneto, G.; Porcar, L.; Hellsing, M. S.; Rennie, A. R.
Manuscript

- IV Polymeric smart coating strategy of titanium implants**
Berts, I.; Ossipov, D.; Fragneto, G.; Frisk, A.; Rennie, A. R.
Manuscript

Reprints were made with permission from the respective publishers.

Papers not included in this thesis

- V Studying various modes of protein adsorption to polymer-functionalized surfaces by neutron reflectometry**
Schneck, M.; Berts, I.; Halperin, A.; Daillant, J.; Fragneto, G.
Manuscript

- VI The swelling of hyaluronan films as a function of humidity**
Dennison, A.; Berts, I.; Brucas, R.; Rennie, A. R.
Manuscript

Contents

1	Introduction	11
1.1	Structure-biology relationships	11
1.2	The interest in hyaluronan	12
1.2.1	HA cross-linking and gel formation	13
1.2.2	HA on surfaces	14
1.3	HA interactions with ions, particles and proteins	15
1.3.1	Ionic interactions	15
1.3.2	HA with particles	15
1.3.3	Protein interactions	16
2	Sample preparation and characterization	19
2.1	Materials	19
2.1.1	Polymers	19
2.1.2	Particles	20
2.1.3	Proteins	20
2.2	Bulk gels, solutions and dispersions	21
2.2.1	Cross-linking reactions	21
2.2.2	Rheology	22
2.2.3	Core-shell	22
2.3	Surface samples	23
2.3.1	Silica and sapphire surface depositions of hyaluronan	23
2.3.2	Titanium oxide surfaces and in-situ deposition of hyaluronan	24
2.3.3	Adsorption of proteins on surface-tethered hyaluronan	25
2.3.4	Surface characterization techniques	25
3	Techniques and data interpretation	27
3.1	Neutron scattering in soft matter	27
3.2	SANS	30
3.2.1	Introduction	30
3.2.2	Data interpretation	31
3.3	Neutron reflectometry	31
3.3.1	Introduction	31
3.3.2	Data interpretation	33

4	Results and discussion	35
4.1	Inhomogeneities in gels and composites.....	35
4.2	Density profiles of grafted and adsorbed HA	38
4.3	Interactions of HA with ions and proteins	42
5	Concluding remarks and future perspectives.....	49
6	Acknowledgements.....	51
7	Svensk sammanfattning	53
8	References	56

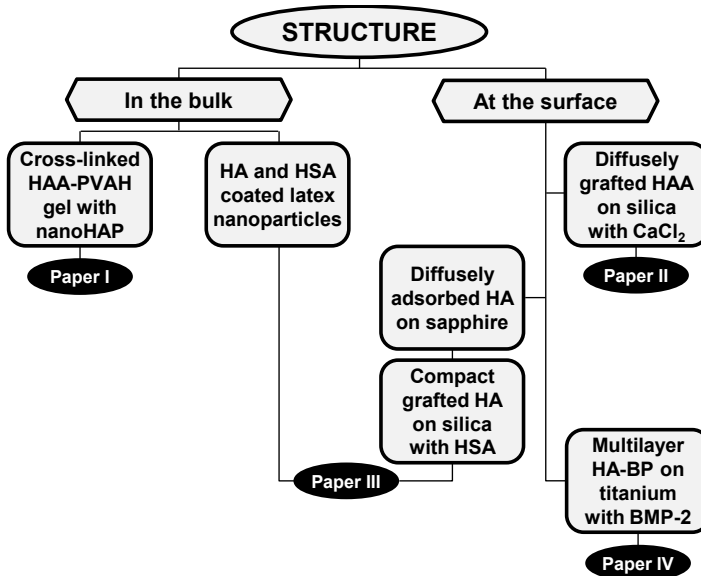
Abbreviations

BMP-2	Bone morphogenetic protein-2
BP	Bisphosphonate
EDC	1-Ethyl-3-(3-dimethylaminopropyl) carbodiimide hydrochloride
HA	Hyaluronan
HA-A	Aldehyde-modified hyaluronan
HA-BP	Hyaluronan containing bisphosphonate groups
HA-BP-H	Bisphosphonate- and hydrazide-modified hyaluronan
HA-H	Hydrazide-modified hyaluronan
HSA	Human serum albumin
NanoHAP	Nano-sized hydroxyapatite particles
pI	Isoelectric point
PVA-H	Hydrazide-modified polyvinyl alcohol
QCM	Quartz crystal microbalance
SANS	Small-angle neutron scattering
Sulfo-NHS	N-hydroxysulfo-succinimide
XPS	X-ray photoelectron spectroscopy

Scope of the thesis

Hyaluronan is a valuable material with versatile applications in the biomedical industry. This dissertation focuses on a structural investigation of hyaluronan in the bulk and at interfaces, using mainly neutron scattering techniques. Knowledge about the structure can be related to the physical properties of biomaterials and improve the future exploitation of hyaluronan as a biomaterial.

In **Paper I**, studies of cross-linked bulk gels and gel-particle composites with small-angle neutron scattering are described. The correlation lengths in these gels were related to their viscoelastic properties. In addition, the particle arrangements are discussed. **Paper II** presents an investigation of surface grafted hyaluronan at a solid-liquid interface with neutron reflectivity. The conformation was investigated in the presence and absence of calcium ions. In **Paper III**, the interaction of hyaluronan with albumin on various surfaces is described. In **Paper IV**, the adsorption and desorption of bone morphogenetic protein-2 on hyaluronan coated titanium surfaces is described. These studies altogether are presented in the **Scheme** below.



Scheme. Schematic presentation of the topics covered in this dissertation.

1 Introduction

Hyaluronan, or hyaluronic acid, is one of nature's most fascinating and versatile macromolecules. It exists in all vertebrates and is one of the main components of the extracellular matrix, synovial fluid, and vitreous humor. Hyaluronan plays an important role in many biological processes and has desirable viscoelastic properties. It is biocompatible and biodegradable, hence having a high application value in the areas of tissue engineering, drug delivery, and viscosupplementation.

This dissertation is mainly based on structural studies of hyaluronan in the bulk and at interfaces. The aim of the work is to describe both the bulk gel structure and the conformational arrangement of hyaluronan at solid-liquid interfaces. Small-angle neutron scattering and neutron reflectivity are the two main techniques used in this work to investigate the nanostructure of hyaluronan in its original, hydrated state. The knowledge from this work should eventually help the design and preparation of future biomaterials and coatings for biomaterials.

1.1 Structure-biology relationships

For biomolecules, structure is usually related to function.¹ This raises questions as to how one determines and then describes the structure. A structure is not only defined by the molecular formula but also by the macromolecular arrangement, for example the folding of a polypeptide chain or the packing of a semi-rigid polysaccharide. For dilute polysaccharide solutions and gels, the packing is affected by their chemical modifications and the interactions with the surrounding medium, as well as the molecules dissolved in the medium. A number of techniques exist to investigate structure in soft condensed matter. However, finding one that provides sufficient detail without altering the native conditions of the samples is not completely straightforward. A section from the work of Chen et al.^{2,3} nicely states this point: 'Currently hyaluronan-based medical products are mostly classified as medical devices, utilizing the physical attributes of hyaluronan to achieve their intended functions. No doubt when the biology of hyaluronan becomes better known, applications will also be developed to utilize its biological function.'

For bulk gels made of hyaluronan, it is optimal to study the structure in its natural state, meaning not frozen or swollen. This requirement rules out cryo-scanning and transmission electron microscopy techniques, as well as swelling experiments based on rubber-elasticity theories which correlate the structure with the viscoelastic properties. The bulk structure is related to the stability of the gel, as well as the ability of the gel to incorporate particles and molecules and their subsequent release. These properties depend on the distances between the cross-links within the gel.

The study of the structure and conformation of surface-tethered hyaluronan would be ideally performed at an aqueous interface, which is very rare in literature.⁴ Many surface immobilization techniques exist for hyaluronan. However, these surfaces are commonly characterized by microscopy techniques, fluorescence measurements, contact angle measurements, ellipsometry, and spectroscopic techniques. Typically one can obtain the chemical composition, the thickness, and the absorbed mass from these measurements, while the information about the hydrated structure at the interface is not accessible. The interfacial structures are significant for the biological function and biocompatibility of a material as it is in immediate contact with the biological medium. In such cases, the surface structure governs the biological response.⁵ Studies have shown that different chain lengths of a polymer affect the ability of a surface to resist protein adhesion.⁶ Other responsive polymer coatings that influence the biotechnological and biomedical applications have also been reviewed.⁷

Neutron scattering techniques are suitable for investigating size-ranges from one to a few hundred nanometers, which is the size-range for most biological structures. These techniques are also chosen because they allow in-situ studies, the possibility for highlighting parts of interest of a system, and because they are non-destructive. Details about this will be discussed in chapter 3. The structural properties of hyaluronan investigated is then related to the physical properties of the material and discussed for their possible use in the field of biomaterials.

1.2 The interest in hyaluronan

Hyaluronan, HA, or sodium hyaluronate, was first isolated from bovine vitreous humor in the 1930s and described as a high molecular mass mucopolysaccharide.⁸ Since then it has been identified as a linear, non-sulfated glycosaminoglycan, consisting of N-acetyl-D-glucosamine and D-glucuronic acid.⁹ The repeating unit is a disaccharide with a molecular mass of 401 g mol^{-1} . The structure is shown in **Figure 1.1**. The chain length, or the molecular mass, varies from a few thousand up to 2–5 MDa.^{10, 11} HA is commonly harvested from cultures of a bacterial strain (*Streptococcus zooepidemicus*).¹²

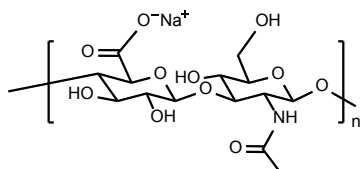


Figure 1.1. The repeating unit of sodium hyaluronan, which is the salt form of HA under physiological conditions.

HA is present in tissues and body fluids of all vertebrates. The highest concentrations in humans are found in skin, synovial fluid, in the umbilical cord and in the vitreous humor.¹³ It is also one of the major components of the extracellular matrix. HA is an anionic polysaccharide playing an important role in biological processes. It is involved in maintaining the osmotic balance and reducing friction in tissues.¹⁴ It also contributes to mediating and modulating cell adhesion, participates in cell mobility, as well as cell development, tumor metastasis, and inflammation.¹⁵⁻¹⁷ HA has been widely used in ophthalmology and rheumatology for the last 40 years,¹⁸⁻²¹ and it has become one of the major compounds envisaged for future biomaterials. However, in spite of these widespread uses and medical applications, the way it acts is till poorly understood.²² It is therefore essential to study the structure and conformation of HA in different environments, as well as the interaction of this material with other biomolecules.

1.2.1 HA cross-linking and gel formation

HA polymers can be chemically modified with groups that can cross-link to form a three-dimensional hydrogel. These hydrogels, when compared with highly concentrated HA solutions, form a more stable scaffold with much improved viscoelastic properties. They also use much less material. Several strategies could be applied for the modification of the carboxylic acid and alcohol groups on HA, including carbodiimide-mediated, diepoxy, aldehyde, divinyl sulfone, photo-cross-linking and reversible disulfide cross-linking.^{4, 23-25}

The study described in this dissertation addresses the hydrazone chemoselective cross-linking between two functional groups; aldehyde and hydrazide. The hydrazone bond created by this reaction is shown in **Figure 1.2**. The HA molecule modified with aldehyde functionalities (HA-A) can form a gel when mixed with a polyvinyl alcohol polymer modified with hydrazide functionalities (PVA-H).²⁶⁻²⁹ The product of this reaction is a hydrogel with a structure that is discussed in **Paper I**. Recently HA modified with hydrazide groups (HA-H) or dual-functionalized HA with both hydrazide and bisphosphonate groups (HA-BP-H) have become available.³⁰ Bisphosphonate groups (BPs) are well-known drugs for the treatment of osteoporosis and osteolytic bone diseases.³¹ BP alone has also been suggested as an adjuvant

to anticancer agents for treatment of bone metastasis.³² The dual-functionalization can hence provide cross-links as well as attach bioactive groups to the HA backbone. The use of BP-modified HA is further discussed in **Paper IV**. The structures of these functional groups are presented in chapter 2.1.1.

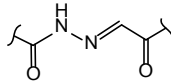


Figure 1.2. The hydrazone formation created by an aldehyde group and a hydrazide group during cross-linking.

The cross-linked hydrogel has been shown to be biocompatible. Previous work has also confirmed that these gels can mediate delivery of ceramic particles and growth factors to induce local bone formation subcutaneously and subperiosteally.^{26, 33} Studying these gel structures with small-angle neutron scattering has its advantages as the technique allows the study of the gel in its original state, without any alteration of its structure.

1.2.2 HA on surfaces

Surface modification of implant materials and devices with HA is a growing field.⁴ The trend of research is moving away from biopassive surfaces towards the third generation biomaterials that combine surface bioactivity with biodegradability.³⁴ These biomaterials should be able to stimulate specific cellular responses as well as undergo a progressive degradation while new tissue regenerates. The rationale for HA coating is the exploitation of the bioinert nature of HA, which can be converted into a bioactive surface by attachment or incorporation of bioactive proteins or peptides.³⁵ HA together with other molecules, for example aggrecan, are also known to have lubricating properties on surfaces.³⁶ HA has been used as a biomimetic coating to prevent protein adsorption on implantable sensors, as well as to reduce blood platelet deposition on stents.³⁷⁻³⁹

In many biological applications, it is the interfacial behavior of a polymer that determines the particular use. This is the reason why it is of great importance to characterize the structure and interactions of polymers at surfaces and interfaces.⁴⁰ As stated in a review about engineering of biomaterials surfaces by hyaluronan: ‘... for all the complexity and peculiarities of interactions involving HA, proper surface chemistry characterization can be found only in a small number of the cited papers, and that direct or indirect information, or even just speculation, on the structure and conformation of surface-linked HA at the aqueous interface is even more rare.’⁴ This statement contributes to the motivation for the study of surface-tethered HA and its interactions at a solid-liquid interface using neutron reflectivity.

1.3 HA interactions with ions, particles and proteins

Another aim for the present work has been to investigate the interactions between hyaluronan and other substances. It is useful to understand the changes in the conformation and properties of HA in simulated physiological environments, e.g. in the presence of ions, nanoparticles and proteins.

1.3.1 Ionic interactions

Ionic interactions are important processes as charged polysaccharides are highly sensitive to changes in ionic strength and concentration. HA is a semi-flexible polymer with a random coil structure.⁴¹ It is highly hydrophilic and can incorporate large amounts of water, which gives HA a unique viscoelastic and swelling behavior. Due to such properties, HA acts well as a lubricant and a shock absorber, either in dilute solution or as cross-linked network.⁴² The flexibility of HA chains is, however, very much dependent on the surrounding ionic strength.⁴³

The influence of calcium was investigated as it is the most abundant metal in the human body. It is present at high concentrations in serum, extracellular fluid, and in bones. In serum the Ca^{2+} concentration varies between 2.1–2.9 mM,⁴⁴ and approximately 0.5 mol of calcium are exchanged between bones and the extracellular fluid over a period of 24 hours.⁴⁵ The calcium homeostasis in the extracellular fluid is regulated by calcitonin-secreting cells.⁴⁶ The ability of cells to secrete calcium, combined with the sensitivity of HA to calcium allows many cell-mediated modifications of the extracellular matrix.⁴⁷

Calcium ions have well-known effects on polyelectrolytes such as HA.^{42, 48} These ions act as inter-chain ionic cross-linkers between anionic polyelectrolyte chains.⁴⁹ In this dissertation, we have studied the influence of calcium ions on diffusely grafted HA-A, described in **Paper II**. Calcium was also used to trigger the release of proteins adsorbed on surface-tethered HA layers and this is discussed in **Paper IV**.

1.3.2 HA with particles

Particles of various sizes are often added to polymeric scaffold materials to create composite materials.⁵⁰ These particles act as reinforcing agents to hydrogels to improve their structural and mechanical properties.⁵¹

Bone is a mineralized tissue that is composed of collagen fibers, proteoglycans and numerous non-collagenous proteins. All of these form an organic matrix that is calcified by calcium phosphate minerals.⁵² Hydroxyapatite is a form of calcium apatite with the formula $\text{Ca}_{10}(\text{PO}_4)_6(\text{OH})_2$. It is one of the most important inorganic constituents of biological hard tissues and often used as bone tissue substitutions.^{53, 54} Nano-sized hydroxyapatite particles

(nanoHAP) were used in the study of HA hydrogel composites,⁵⁵ described in **Paper I**.

The latex nanoparticles are used as a model for colloidal drug carriers for tissue-specific drug targeting after intravenous application.⁵⁶ Injectable polymeric nanoparticle drug carriers have the ability to revolutionize disease treatment via controlled drug delivery.⁵⁷ However, proteins present in the blood serum can quickly bind to these nanoparticles, allowing recognition and removal of these particles by the immune system. Several methods have been developed to mask or camouflage the nanoparticles such as adsorption or grafting of polymers to the surface of the particles.⁵⁸⁻⁶⁰ **Paper III** describes a co-adsorption study of a serum protein together with HA. This can give insights into the adsorption processes for materials used as colloidal drug carriers.

1.3.3 Protein interactions

Despite the apparent simplicity of the primary structure of HA, this molecule can exert multiple, often molecular mass-dependent, biological effects not only through its physicochemical properties but also through direct interactions with proteins and cell surface receptors.⁴ What are the bases that control the interaction between HA and other biomolecules?

Protein adsorption on artificial implant surfaces is usually the first event that triggers biological responses. In many cases proteins and peptides are used to coat implant surfaces to modify the surface properties, e.g. to improve cell adhesion.^{61, 62} Studies show that using adhesive proteins and peptides enhances bone repair and orthopedic implant integration.⁶³ In contrast, many protein adhesion processes are undesirable as they cause thrombus formation and foreign body reaction. To avoid such adverse events, coatings based on surface-tethered polymers or proteins (commonly HSA) have been designed to prevent non-specific adsorption and subsequent microbial adhesion.^{64, 65}

In this dissertation, the focus lies on human serum albumin (HSA) and bone morphogenetic protein-2 (BMP-2). The structures of HSA and BMP-2 are shown in **Figure 1.3**. HSA is the most abundant protein in blood plasma and plays a key role in the transport of fatty acids, metabolites and drugs. HSA widely serves as a good model protein for the study of protein adsorption due to its low cost, high abundance and stability. HSA is extensively studied and well-described in literature.⁶⁶⁻⁶⁸

The pI of HSA is 4.7.⁶⁷ HA has a pK_a value of about 3.0.⁶⁹ Electrostatic interactions between HA and HSA are expected in the pH range between 3 and 4.8 during which the two molecules will be oppositely charged. However, other physical interactions might also exist. A solution at pH 7.4 containing both HSA and HA with their respective concentrations close to those of synovial fluid^{70, 71} showed shear thinning properties (described in **Paper III**).

The interactions of HSA with HA have been studied at various interfaces. In this dissertation the co-adsorption of HSA and HA on latex particles and the HSA adsorption on surface-tethered HA are discussed.

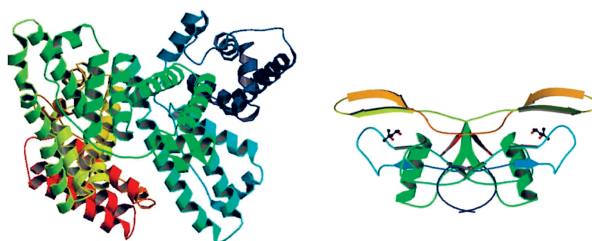


Figure 1.3. Crystal structure of HSA⁷² (left) and BMP-2⁷³ (right), images are taken from RCSB Protein Data Bank.⁷⁴

BMP-2 is a growth factor commonly used to promote bone regeneration on implant surfaces.⁷⁵⁻⁷⁷ The efficiency of BMP-2 depends strongly on the method of delivery. It does not have any osteogenic effects when adsorbed directly on a bare titanium implant surface.⁷⁶ However, it has been shown that BMP-2 imbedded in an HA scaffold has promising osteoinductive effects and the degradation behavior of the scaffold was well-controlled.²³ Although BMP-2 can promote robust bone formation, it also induces adverse clinical effects that include cyst-like bone formation and significant soft tissue swelling. At concentrations below $10 \mu\text{g ml}^{-1}$ the BMP-2 is not effective, while at concentrations above $150 \mu\text{g ml}^{-1}$ cyst-like bony shells filled with adipose tissue is observed. Significant increase in bone volume without any adverse effects is only seen for BMP-2 at a concentration above $30 \mu\text{g ml}^{-1}$.⁷⁸ Therefore, BMP-2 is often administered using carrier matrices to maintain a controlled concentration at the treatment site.⁷⁹ The concentrations found in humans are, however, much higher ($1500 \mu\text{g ml}^{-1}$).⁷⁸

Promotion of binding or mineralization between bone tissue and the implant is common processes today to increase bioactivity in bone repair and fixation of prostheses.⁸⁰ The adsorption and desorption of BMP-2 on HA-functionalized titanium surfaces is described in **Paper IV**.

2 Sample preparation and characterization

This section describes the preparation of HA bulk and interface samples and the pre-characterization techniques conducted prior to the neutron scattering experiments.

Modified polymers were used in the cross-linking reactions to form chemically cross-linked bulk gels. Both modified HA and native HA has been used for the grafting and adsorption experiments at solid-liquid interfaces. Different concentrations, immobilization reactions and deposition protocols were used. The surfaces involved were the native silicon oxide on the (111) face of silicon crystals, the native titanium oxide on the metallic titanium sputtered on these silicon crystals, and sapphire crystals (Al_2O_3).

The adsorption of HSA on latex particles and the co-adsorption of HSA and HA on latex particles is discussed in section 2.2.3. The protein interaction on surface-tethered HA is discussed in section 2.3.3. These were studied with SANS and neutron reflectometry in-situ.

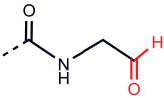
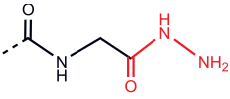
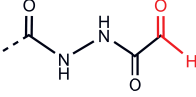
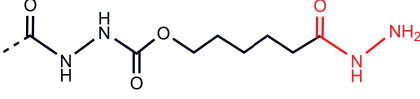
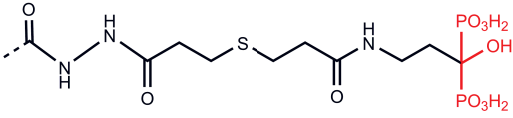
The pre-characterization techniques conducted were rheology, X-ray photoelectron spectroscopy, ellipsometry, X-ray reflectivity, and quartz crystal microbalance. Performing these prior to the scattering experiments is essential to confirm the quality of the samples and to obtain knowledge about the samples. Furthermore, information from these techniques enabled correct interpretation of the scattering data using appropriate models.

2.1 Materials

2.1.1 Polymers

The chemically modified polymers are listed in **Table 2.1**. The synthesis of HA-A for the study described in **Paper I** and **Paper II** is described in literature.²⁶ The PVA-H was prepared according to a previously published protocol.²⁹ The synthesis of HA-A, HA-H and the dual-functionalized HA-BP-H used for the study described in **Paper IV** was by Ossipov et al. and Yang et al.^{30, 81} The native HA used in **Paper III** had various different molecular masses that span from 51 kDa to 1.47 MDa. Native HA polymers were purchased from Shiseido and Lifecore Biomedical (medical grade).

Table 2.1. The chemically modified HA with their respective physical properties. The functional groups are indicated in red.

Name	Molecular mass and degree of modification	Structure of the modified group	Paper
HA-A	180 kDa 6%		I, II
PVA-H	14 kDa 9%		I
HA-A	130 kDa 5%		IV
HA-H	130 kDa 10%		IV
HA-BP	130 kDa 15%		IV

2.1.2 Particles

The nanoHAP are non-spherical particles discussed in detail in the paper by Hu et al.⁵⁵ These particles have been studied with transmission electron microscopy and dynamic light scattering which confirmed that the particles were grain-like and had a size distribution with an average diameter of 20 nm and 20% polydispersity.⁵⁵

The latex made of deuterated polystyrene (C_8D_8) are spherical particles with radius $362 \pm 42 \text{ \AA}$. The synthesis has been described by Hellsing et al.⁸²

2.1.3 Proteins

HSA is a monomeric polypeptide with a molecular mass of 66 kDa. In solution it adopts a prolate ellipsoidal shape with $a = 70 \pm 2 \text{ \AA}$ and $b = 20 \pm 1 \text{ \AA}$.⁸³ The three-dimensional crystal structure shows, however, that it has a heart-shaped asymmetry. The albumin content in the synovial fluid varies both between species and between different limb joints.⁸⁴ HSA of 15 mg ml^{-1} was taken as a model to mimic the concentration in synovial fluid during the rheology measurements. The surface interaction experiments used a concen-

tration range between 1–5 mg ml⁻¹. HSA used in this study was purchased from Sigma-Aldrich (A3782).

BMP-2 is a 26 kDa homodimer with dimensions 70 Å × 35 Å × 30 Å. It has a butterfly-like shape where the middle, thinnest part is only about 10 Å thick.⁷³ The concentrations used in this study were 7.5 µg ml⁻¹ and 37.5 µg ml⁻¹. These concentrations were selected to be comparable to the concentration range used in literature.^{78, 85-87} BMP-2 was purchased from InductOs.

2.2 Bulk gels, solutions and dispersions

2.2.1 Cross-linking reactions

Bulk gels described in **Paper I** were prepared through a rapid mixing of HA-A and PVA-H components shortly before filling the sample holders while the material still had a fluid-like behavior. The concentrations of each component were calculated to have a 1:1 ratio of the respective cross-linking groups. The final total polymer concentrations of the gels were 5, 15 and 30 mg ml⁻¹. The nanocomposite samples were prepared with the 15 mg ml⁻¹ gel matrix. The particles were dispersed in the HA-A component prior to cross-linking as the HA-A solution is sufficiently viscous to prevent sedimentation of the particles. During cross-linking the mobility of the nanoHAP is hindered, leading to the particles being frozen in the 3D gel network. Samples were contained in 1 mm path length fused quartz cells for scattering measurements, see **Figure 2.1**. The cross-linked gel samples are completely transparent to light. Earlier work indicated that the refractive index of these gels (1.336–1.337) are very similar to those of water and balanced salt solutions (1.333).⁸⁸ The nanocomposite samples have increased mechanical stability but are not transparent to light.

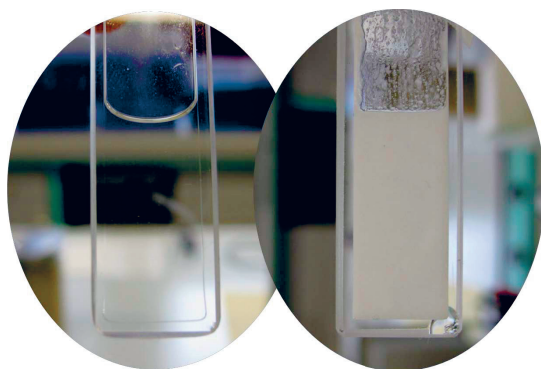


Figure 2.1. Gel sample to the left and nanocomposite sample to the right in 1 mm path length fused quartz samples cells.

2.2.2 Rheology

Rheology is the study of deformation and flow of matter resulting from an applied force. Hydrogels are viscoelastic which means they possess aspects of the behavior of both solids and liquids.⁸⁹ Oscillatory shear rheology measurements on the cross-linked HA-A and PVA-H gels of three concentrations related their macroscopic properties with their nanostructure. The viscoelastic properties described by the storage and loss moduli, are in turn dependent on the connectivity between the polymers in the gel.⁹⁰ This is discussed in **Paper I**.

Physical entanglements of large macromolecules can also cause viscoelastic behavior. Oscillatory shear rheology as well as viscosity measurements were performed on HA solutions and HSA solutions, as well as their mixtures at different pH. The concentration of HA (3 mg ml^{-1}) and HSA (15 mg ml^{-1}) used in this study were chosen to mimic the concentration of the respective components found in synovial fluid.^{70, 71} The pH values chosen in this study are related to the pI of HSA, as well as the physiological pH of 7.4. Details are discussed in the supplementary information to **Paper III**.

2.2.3 Core-shell

The core-shell assembly of proteins on nanoparticles usually has the core deuterated. It is then possible to make the core invisible to neutrons by adjusting the scattering length density of the aqueous medium through the $\text{H}_2\text{O}-\text{D}_2\text{O}$ ratio, in the meanwhile highlighting the protein corona.⁹¹ The particles used in this study were deuterated polystyrene latex which, if dispersed in D_2O , are almost invisible to neutrons. The adsorbed HSA and the co-adsorbed HSA and HA mixture were modeled with a core-shell function where the shell has a uniform thickness. A schematic summary of the adsorption on latex particles is shown in **Figure 2.2**.

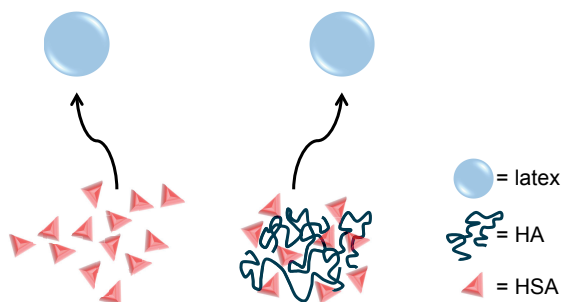


Figure 2.2. Summary of the HSA adsorption and the HSA and HA co-adsorption on latex particles.

2.3 Surface samples

2.3.1 Silica and sapphire surface depositions of hyaluronan

Both silica and sapphire are suitable substrates in reflectivity studies as they are transparent to neutrons and can be polished into smooth surfaces. Silica surfaces can be modified to have different surface functionalizations using silane chemistry,⁹²⁻⁹⁵ and in this work, the surfaces were prepared to be optimized for HA immobilization.^{35, 96, 97} Different pI values (from about 5 to 9) for sapphire crystals have been reported in the literature.⁹⁸⁻¹⁰¹ This suggests that the pI depends on the crystal face and may be different for amorphous alumina.¹⁰² However, using solutions of pH between 3 and 5 should enable the adsorption of HA on sapphire. The surface dimensions were $50 \times 50 \text{ mm}^2$. The surfaces underwent thorough cleaning before measurement and deposition. The cleaning procedure involved sonication in chloroform, acetone, ethanol and water in turn (5 min each), followed by a UV-ozone treatment for 30 min. This procedure provides highly hydrophilic silica or sapphire surfaces.

Two types of polymer grafting on silica are covered in this dissertation, Schiff base reaction followed by reductive amination, and carbodiimide-mediated condensation. In both cases an amine-terminated silane was used to modify the surface to contain surface amines. Both (3-aminopropyl)-trimethoxysilane and (3-aminopropyl)-diethoxymethylsilane have been used. The first one is described in **Paper II** and the second in **Paper III**. Both give the surface a primary amine functionalization, required for further HA immobilization.

As discussed in **Paper II**, the reaction between the aldehyde on HA-A and the amine produces an imine bond which is reduced by sodium cyanoborohydride to a stable amine bond.^{103, 104} Two strategies were used, single- and two-stage deposition. During the single-stage deposition the aminated surface was immersed in a 10 mg ml^{-1} HA-A solution, the sodium cyanoborohydride was added and the reductive amination was allowed to occur. During the two-stage deposition the aminated surface was immersed twice in a 5 mg ml^{-1} HA-A before the reduction reaction. The grafted HA-A layer produced by both deposition protocols was studied with ellipsometry and neutron reflectivity.

The carbodiimide-mediated condensation reaction used 1-ethyl-3-(3-dimethylaminopropyl) carbodiimide hydrochloride (EDC) as a water-soluble, zero-length cross-linking agent to couple carboxyl groups of the HA repeating unit to surface-anchored primary amines.¹⁰⁵ EDC reacts with the carboxylic acid groups to form an unstable reactive *O*-acylisourea intermediate. This intermediate may react with an amine, but it is also very susceptible to hydrolysis, making it short-lived in an aqueous solution. The addition of

N-hydroxysulfo-succinimide (Sulfo-NHS) stabilizes the intermediate by converting it to an amine-reactive Sulfo-NHS ester, thus increasing the efficiency of the EDC-mediated coupling reaction.¹⁰⁵⁻¹⁰⁷ EDC condensation is one of the most frequently used methods for HA immobilization according to the review by Morra.⁴ The grafted HA samples were measured with ellipsometry and neutron reflectivity, as discussed in **Paper III**.

The sample holder used for neutron reflectivity experiments is shown in **Figure 2.3**. The design allows for fluid exchange while maintaining the hydrated state of the interface. This figure is modified from Hellsing et al.¹⁰⁸ The grafted samples on the silicon substrates were thoroughly rinsed to remove any unbound material before mounting on the sample holder. The in-situ adsorbed samples are injected through the fluid inlet onto a clean substrate, followed by rinsing with pure solvent before measurement or further injections.

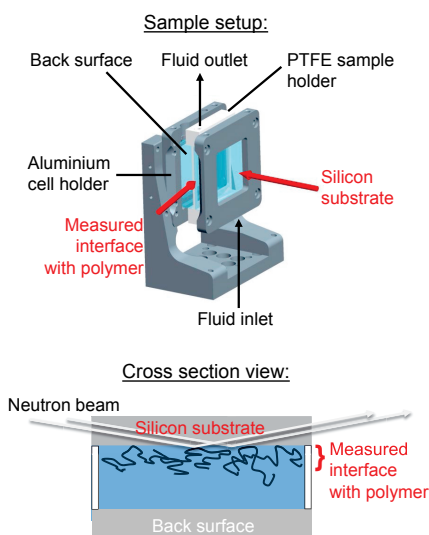


Figure 2.3. The sample cell setup¹⁰⁸ for neutron reflectivity experiments (top) and the cross section view of the measured polymers at a solid-liquid interface (bottom).

2.3.2 Titanium oxide surfaces and in-situ deposition of hyaluronan

Sputtering metallic titanium onto polished silicon surfaces provides smooth surfaces suitable for reflectivity as well as a good model for titanium implants used in orthopedics. The surfaces were $50 \times 50 \text{ mm}^2$ in size with the outer layer consisting of titanium oxide, which was created on top of the metallic titanium layer when the surfaces were exposed to the atmosphere.

The polymers were adsorbed on the surface using a layer-by-layer deposition in-situ. HA-H was alternated with HA-A (four times each) to form an

HA gel on the surface. The mechanism is the hydrazone cross-linking as described previously in chapter 1.2.1 and 2.2.1. An HA-BP gel could also be formed by replacing the HA-H with HA-BP-H. BP groups can facilitate the binding to titanium through Ti-O-BP bonds. All HA solutions used in this study had a concentration of 1 mg ml^{-1} .

2.3.3 Adsorption of proteins on surface-tethered hyaluronan

Studies of protein interaction on surface-tethered HA are described in **Paper III** and **Paper IV**. The proteins were injected to the HA surfaces and the changes were followed by neutron reflectivity. A summary of the protein interaction of HA on surfaces is illustrated in **Figure 2.4**.

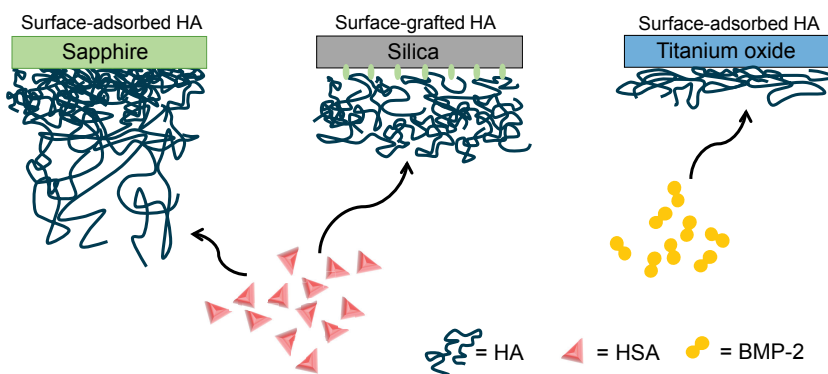


Figure 2.4. Summary of the protein interaction of HA with different surfaces studied with neutron reflectivity.

2.3.4 Surface characterization techniques

Ellipsometry measurements were conducted prior to the neutron reflectivity measurements for all samples that were not made through in-situ deposition. This measurement verifies the uniformity and the thickness of the oxides on the substrates as well as the grafted layers. The technique is based on the changes in the polarization of light upon reflection from a surface.¹⁰⁹ The characterization is performed at the solid-air interface, meaning that the measured polymer layer is not immersed in water as during the neutron reflectivity experiments. However, it is possible to follow the grafting procedure and relate the dry collapsed polymer layers to the hydrated structures between different samples.

X-ray photoelectron spectroscopy (XPS) was performed on the silica surfaces after the deposition of the surface amines (using silanes) to confirm the existence and the ratio of nitrogen atoms (from the amines) compared to the silicon atoms. This technique determines the elemental composition and

chemical binding from peak intensities and the chemical shifts, and is hence utilized to analyze the relative amounts of different chemical species.¹¹⁰

X-ray reflectivity is a good complementary technique to neutron reflectivity. The measurements were conducted on laboratory X-ray reflectometers. The grafted samples were measured with X-ray reflectivity before the neutron reflectivity experiments to control the sample quality. Measurements were also made on the titanium sputtered surfaces to confirm the thickness and uniformity of the sputtered layer.

Quartz crystal microbalance (QCM) is an ultrasensitive weighing device, which is based on the frequency shifts of a freely oscillating sensor. It determines the total oscillating mass.^{111, 112} If the adsorbed layer is thin and rigid one can relate proportionally the decrease in frequency (Δf) to the mass of the film according to Sauerbrey relations.^{113, 114} The mass m of the adhering layer is $\Delta m = C / n \Delta f$, where C is the mass sensitivity constant of the crystal ($17.7 \text{ ng Hz}^{-1} \text{ cm}^{-2}$ for a 5 MHz quartz crystal), and n is the frequency overtone number (3, 5, 7, 9 and 11 were measured in this work). Further descriptions of this technique can be found in the dissertation by Höök et al.¹¹⁴ This technique is widely used to study protein adsorption processes in liquid media.¹¹⁵⁻¹¹⁹

3 Techniques and data interpretation

3.1 Neutron scattering in soft matter

Neutron scattering is described by Roger Pynn as a method for ‘seeing inside matter’.¹²⁰ Generally, neutron scattering is a family of techniques in which neutrons are used as probes to determine the structural and dynamical properties of materials by measuring the change in direction and energy of the neutron after interacting with a sample.¹²¹ This dissertation has its focus on the study of biology-related materials using primarily small-angle neutron scattering and neutron reflectometry. Here, the neutrons are scattered elastically, which provides the structural information in soft matter. This work does not include inelastic or quasielastic scattering techniques such as time-of-flight spectroscopy, back-scattering, and spin echo, which determine dynamic properties of materials.

The advantages of using neutrons as probes are many. Being electrically neutral (without charge), neutrons interact with the nuclei of atoms. This means that the scattering from different isotopes of a given atom (which are defined by the number of neutrons in the nucleus) can differ significantly. Neutrons, just like light, have the characteristics of both particles and waves. The amplitude of the scattering from a nucleus is defined by the scattering length b , whose magnitude describes the strength of the neutron-nucleus interaction. The total probability of scattering of a neutron by a nucleus is described by the scattering cross section σ . This can be thought as the hypothetical surface area of the target. The scattering cross section is made up by both the coherent and the incoherent cross sections. For elastic scattering, coherent scattering arises from interference between the neutrons scattered from different nuclei which yields the structural information about a sample. The incoherent scattering usually appears as unwanted background, as there is no interference between waves scattered by the different nuclei. σ_{coh} is related to b such that $\sigma_{\text{coh}} = 4\pi|b|^2$. **Table 3.1** compares the neutron scattering lengths and the coherent cross sections with the equivalent atomic form factors for X-rays f , the last quantity being analogous to the neutron scattering length.¹²⁰⁻¹²³

The difference in the scattering length between hydrogen and deuterium is extremely valuable for the study of hydrogen-containing materials and forms the basis of a method known as contrast variation. For X-ray scattering, as the electrons are being probed, the intensity increases linearly with the atom-

ic number that consequently favors the scattering of heavier atoms. Neutron scattering, on the other hand, is determined by the nuclear structure where the value of b is not proportional to the atomic number, which makes it favorable in the study of biologically relevant samples which contains mostly lighter elements, and where hydrogen could be substituted with deuterium in solvents and in molecules.

Table 3.1. Neutron scattering length b and coherent cross sections σ_{coh} for elements in synthetic and natural biomaterials,¹²⁴ compared with the atomic X-ray form factors.¹²⁵ Values for b and σ_{coh} for all elements (except for ^1H and ^2H) are averaged based on their natural abundance.

Atom	b (fm)	σ_{coh} (fm ²)	$f_{\text{X-ray}}$ (fm) at $\lambda=1.54 \text{ \AA}$
^1H	-3.74	176	2.81
^2H	6.67	559	2.81
C	6.65	555	17.0
N	9.36	1102	19.9
O	5.80	423	22.7
Si	4.15	216	40.2
P	5.13	331	43.2
S	2.85	102	46.0

When probing structures that are larger than single atoms it is useful to calculate the scattering as coming from an average volume. The overall scattering from a molecule arises from the sum of all individual atomic scattering lengths. This quantity, when normalized with their physical volume, is the scattering length density $\rho = \Sigma b / V_m$, where V_m is the molecular volume of the molecular species of interest. **Table 3.2** lists a few substances and their physical properties and scattering length densities ρ .

Table 3.2. Physical properties of materials used in this work, including ρ .

Name	Formula	Molecular mass (g mol ⁻¹)	Density 25°C (g cm ⁻³)	ρ (10 ⁻⁶ Å ⁻²)
Water	H ₂ O	18	0.997	-0.56
Heavy water	D ₂ O	20	1.1	6.35
HA repeat unit	C ₁₄ O ₁₁ H ₂₀ NNa	401	1	1.43-2.20
HSA	C ₂₉₃₆ H ₄₆₂₄ N ₇₈₆ O ₈₈₉ S ₄₁	66472	1.36	1.84-3.14
BMP-2	C ₁₁₄₂ H ₁₇₇₀ N ₃₂₀ O ₃₂₇ S ₁₈	25776	1.53	2.11-2.75
NanoHAP	Ca ₁₀ (PO ₄) ₆ (OH) ₂	1004	3.16	4.19-4.51
Deuterated latex	C ₈ D ₈	112	1.13	6.41
Silicon	Si	28	2.33	2.07
Silica	SiO ₂	60	2.20	3.41
Sapphire	Al ₂ O ₃	102	3.89	5.75
Titanium	Ti	48	4.51	-1.95
Rutile	TiO ₂	80	4.27	2.63

Isotopic substitutions in biological samples and sample environments create the desirable contrast to highlight different components strategically. Ergo, it is possible to identify different components in a complex system, for example by using deuterated molecules or particles. Furthermore, as ρ for H_2O and D_2O have different signs, one could strategically prepare solvent mixtures of water and heavy water to achieve the desirable contrast for the matching of a substrate or a constituent.^{126, 127} The principle of contrast variation (or contrast matching) is illustrated in **Figure 3.1** for a SANS experiment. In this example the core-shell particles with either the shell (blue) or core (yellow) are matched to the surrounding medium.

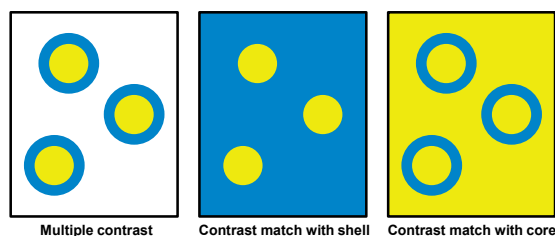


Figure 3.1. Illustrative representation of contrast matching to highlight different components in a complex system.

Neutrons interact weakly with matter through short-range interactions. They are able to penetrate deeply into bulk samples, at the same time being able to access buried interfaces. Furthermore, neutrons do not cause any radiation damage to samples. However, due to the weak interactions, a larger sample size is needed to increase the scattering signal.¹²⁰ The wavelength (λ) of neutrons for SANS and reflectivity experiments is usually between 1–30 Å, and is comparable to the interatomic spacing. It is therefore an excellent way to investigate the structure of various substances at a mesoscopic scale. Neutron scattering enables studies of samples under realistic conditions in terms of sample environments, i.e. temperature control, flow, in-situ depositions etc. Consequently this makes the technique optimal to study gels, melts, solutions, and dispersions.¹²⁸

This dissertation describes bulk studies that were carried out with SANS, and studies on solid-liquid interfaces were performed using neutron reflectometry.

3.2 SANS

3.2.1 Introduction

Small-angle neutron scattering is the technique of choice for the characterization of structures in the bulk. It covers structures of sizes from a few ångström to the near-micrometer scale.¹²⁸ It is a well-established characterization method to investigate proteins, lipids, polymers, particles and colloidal dispersions.¹²⁹⁻¹³⁴ The crucial feature of SANS that makes it particularly useful for the biological sciences is the previously mentioned contrast matching.

The basic theory of small-angle scattering has been described by Guinier and Fournet,¹³⁵ and the SANS technique by Windsor.¹³⁶ One could illustrate the scattering experiment with **Figure 3.2**. The neutron beam goes through the bulk of a sample and the scattering arises from variations in scattering length density in the sample. The distribution of the scattering intensity $I(Q)$ is usually measured on a two-dimensional area detector, where Q is the momentum transfer vector. $Q = (4\pi/\lambda) \sin \theta$, where λ is the wavelength and 2θ is the scattering angle. $I(Q)$ can be expressed as:

$$I(Q) = N_p V_p (\Delta\rho)^2 P(Q) S(Q)$$

where N_p is the number concentration of the objects that are causing scattering, V_p is the volume of one scattering object, and $(\Delta\rho)^2$ is the difference in scattering length density between the scattering objects and the surrounding medium. $P(Q)$ is a function known as the form or shape factor. It defines the size, shape and the distribution in scattering length density of the studied particle or molecule. $S(Q)$ is the structure factor which describe the correlation between the particles or molecules that are causing scattering. $I(Q)$ has dimensions of $(\text{length})^{-1}$ and is normally expressed in units of cm^{-1} .^{136, 137}

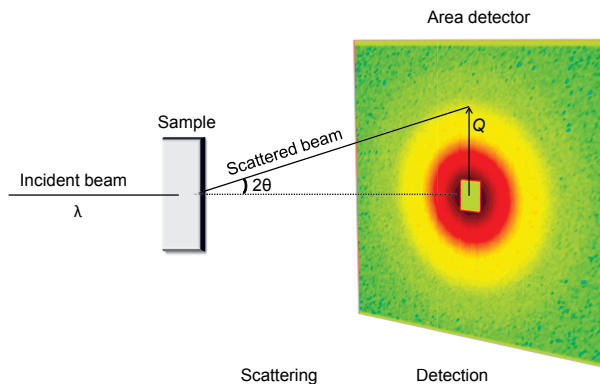


Figure 3.2. A schematic diagram of the SANS technique (not to scale).

The SANS measurements in this dissertation were performed on the D11, D22 and D33 instruments at the Institut Laue-Langevin, Grenoble, France.¹³⁸⁻¹⁴⁰ This technique was used to study cross-linked gels and gel composites containing hydroxyapatite particles, as well as protein and hyaluronan coated latex nanoparticles. Detailed descriptions can be found in **Paper I** and **Paper III**.

3.2.2 Data interpretation

The raw scattering data collected over all Q -ranges are normalized to a fixed number of incident neutrons (same monitor counts), corrected for instrumental and sample cell background, detector pixel non-uniformity, and instant flux. The data are masked for beam stops before finally being merged.^{141, 142} A model for the cross-linked gel structure are derived from the work of Horkay et al.^{143, 144} and Geissler et al.,^{145, 146} and describes the gel being inhomogeneous and consisting of two independent length scales. The fitting was made by Origin Pro. The gel composite system is modeled with SASfit,¹⁴⁷ where the nanoHAP incorporated in the contrast matched gels are treated as clusters that aggregate inside the polymer matrix.

The latex particles and the core-shell model consisting of coated particles are fitted using SASview.¹⁴⁸ SASview allows fitting of complex systems containing several form and structure factors. In **Paper III**, the model consists of protein coated latex particles with a certain degree of aggregation between the coated particles, in combination with an addition term representing protein remaining in solution that was not bound to the latex. The calculation of the protein surface coverage Γ is based on the shell thickness with respect to the protein volume fraction. This is similar as for calculations of Γ of polymers discussed in details in section 3.3.2.

3.3 Neutron reflectometry

3.3.1 Introduction

Neutron reflectometry measures structure and composition of materials at interfaces. An interface is a surface forming a common boundary between two different phases. In this dissertation, the interfaces of interest are those of polymers on an insoluble solid, immersed in a liquid. This technique provides information about the interfacial thickness, roughness and composition. The size range that can be investigated is similar to SANS.^{149, 150} Other similarities are the possibility of deuterium labeling of molecules and contrast variation using solvents of different H₂O and D₂O ratios. Many biologi-

cal soft matter systems at interfaces are studied with neutron reflectometry, such as surfactants, polymers, proteins, and lipids.¹⁵¹⁻¹⁵⁴

These experiments measure reflectivity, which is the ratio of the intensity of the reflected beam I_R , over the intensity of the incoming beam I_I ; $R(Q) = I_R/I_I$, as a function of the momentum transfer vector Q perpendicular to the interface (z -direction). The reflection is specular, which means that the angle of the incoming beam θ_i is the same as the angle of the reflected beam θ_R .^{149, 155} This is illustrated with **Figure 3.3**. The measured reflectivity arises from the difference in refractive index of the bulk phase and the various layers that might be at the surface, and is dependent on the angle and wavelength of the neutrons. The refractive indices n in different materials are related to their scattering length density by the approximate equation $n \approx 1 - (\lambda^2 \rho / 2\pi)$, where λ is the wavelength and ρ is the scattering length density of the material. Although it is possible to express reflectivity with the first Born approximation: $R(Q) \approx (16\pi^2/Q^4) |\rho'(Q)|^2$ where $|\rho'(Q)|^2$ is the Fourier transform of the scattering length density profile normal to the interface,^{149, 155, 156} in practice it is more convenient to calculate reflectivity using a multilayer optical matrix method. This method assumes homogeneous layers parallel to the interface, each with uniform ρ . With this information, a reflectivity profile for a given compositional or density profile can be calculated.^{157, 158}

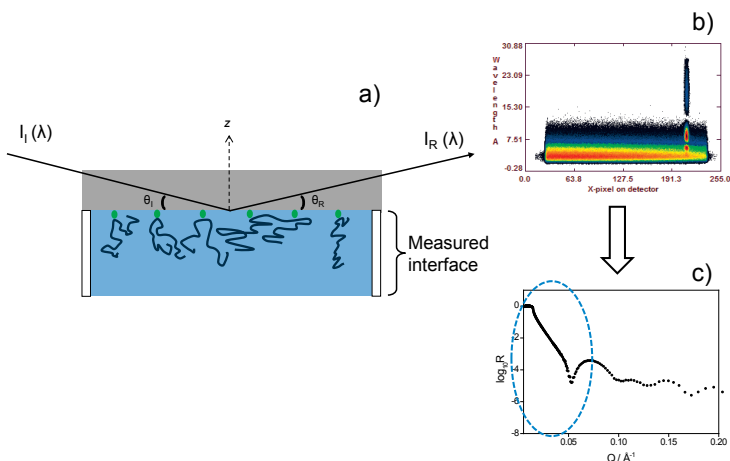


Figure 3.3. Schematic diagram of neutron reflection technique. a) The neutron beam is reflected by the sample. b) A two-dimensional detector shows the signal (for one angle) as a function of wavelength and c) the data after being reduced with COSMOS¹⁵⁹ are displayed as reflectivity as a function of Q .

The neutron reflectivity measurements were performed on the time-of-flight reflectometers D17 and FIGARO at the Institut Laue-Langevin, Grenoble, France.^{160, 161} The data treatment was performed with COSMOS.¹⁵⁹ This technique was applied to study grafted and adsorbed HA on silica, sapphire

and titanium oxide surfaces. The structural changes of the HA layers due to the change of counter-ions or protein adsorption was also studied. Detailed descriptions can be found in **Paper II-IV**.

3.3.2 Data interpretation

Routine analysis of reflectivity data was used to model the interfacial layers with an assigned thickness, roughness and ρ , this was then converted into volume fraction profiles. The programs used in this dissertation are CPROF and WETDOC.¹⁶² Both are able to model multiple contrast data for a single sample, as additional measurements on one sample using a different isotopic composition of the solvent enable one to verify the composition in a layer. Generally, it is useful to assume that the degree of solvent penetration is the same in a layer. However, using solvent with different contrasts will give rise to different ρ for that layer. One can define the scattering length density of one polymer layer ρ_{layer} as $\rho_{\text{layer}} = \sum \phi_i \rho_i$, where ϕ_i is the volume fraction of component i in the layer and ρ_i being the scattering length density of that component. In the case for a two-component system such as a polymer layer in a solution, $\rho_{\text{layer}} = \phi_{\text{polymer}} \rho_{\text{polymer}} + (1 - \phi_{\text{polymer}}) \rho_{\text{water}}$, where ϕ_{polymer} is the volume fraction of the polymer. One could then deduce that $\phi_{\text{polymer}} = (\rho_{\text{layer}} - \rho_{\text{water}}) / (\rho_{\text{polymer}} - \rho_{\text{water}})$.

CPROF differs from WETDOC at the layer most adjacent to the solvent, where CPROF fits a decay profile with options including exponential, linear, parabolic, half-Gaussian, and scaling law functions.¹⁶³ A smooth decay profile is common for proteins and gels at interfaces.¹⁶⁴ The functions define the volume of a component as the sum of a uniform layer and a decay profile. The uniform layer has a thickness t where the volume fraction is constant ϕ_t . The following volume in the decay profile is defined by the type of function one chooses. The molecular surface coverage Γ (e.g. mass per area) is also calculated differently depending on the type of profile, see **Table 3.3**.

Table 3.3. Surface coverage calculations for different profiles.

Profile	Function $\varphi(z)$	a	$\Gamma = \int_0^a \varphi(z) dz$
Exponential	$\varphi(z) = \varphi_t t + \varphi_t e^{-\frac{z}{l}}$	∞	$\varphi_t (t + l) \times d$
Linear	$\varphi(z) = \varphi_t t + \left[\varphi_t - \varphi_t \left(\frac{z}{l} \right) \right]$	l	$\varphi_t \left(t + \frac{l}{2} \right) \times d$
Parabolic	$\varphi(z) = \varphi_t t + \left[\varphi_t \left(1 - \frac{z^2}{l^2} \right) \right]$	l	$\varphi_t \left(t + \frac{2l}{3} \right) \times d$

where the volume fraction $\varphi(z)$ is the volume fraction in the z -direction, φ_t is the volume fraction where the decay starts, t is the layer thickness, l is the

decay length and d is the molecular density. The area per molecule A is obtained from $A = M / (\Gamma N_A)$, where M is the molecular mass and N_A is Avogadro's number.

4 Results and discussion

This dissertation describes studies of the structure of HA hydrogels in the bulk and of HA grafted and adsorbed at interfaces. In addition, the interactions with ions, particles and proteins were studied to investigate the possible structure modifications of HA caused by these interactions. The aim was to relate the structure of HA to the physical properties of future biomaterials or coatings for biomaterials, and further to simulate the interactions in a physiological environment. The results are largely based on models derived from neutron scattering data, where some prior knowledge about the sample is necessary to be able to distinguish different components of the measured signal in order to correctly interpret the data. The knowledge derived could be applied in the preparation of future biomaterial devices.

4.1 Inhomogeneities in gels and composites

Bulk gels consisting of cross-linked HA-A and PVA-H were studied with SANS and rheology as described in **Paper I**. As mentioned in chapter 1, these hydrogels have already shown good biocompatibility, can incorporate particles and growth factors to induce bone formation, as well as showing a controlled degradability.^{26, 165} However, the structure of these gels is not well-known. Parameters that usually characterize a gel network structure include the molecular mass between two neighboring cross-links, the corresponding mesh size, and the effective network density.^{166, 167} These are related to viscoelastic properties of the gel by the theories of rubber elasticity that, for example, can be used to calculate swelling by solvent.^{168, 169} Many gels are very fragile and rupture easily in solvents if they are not constrained. Constraining the gels on the other hand limits the diffusion of solvents into them. The two polymers used in this gelation process also differ in the molecular mass and the cross-linking reaction is completely randomized. These two factors could further complicate the prediction of the structure, which cannot be calculated by a traditional swelling experiment where one has to assume the gels to have a homogeneous network structure.¹⁷⁰

Gels consisting of three different polymer concentrations showed different scattering behavior as well as different viscoelastic behavior. Modeling of the SANS data showed that the gel structure is inhomogeneous, consisting of two length scales, L and Ξ . L describes the mesh size for gels formed by

semi-flexible polysaccharides that exhibit rod-like behaviors.^{143, 171} In literature it is, however, more common to see the mesh size described by ξ ,¹⁷² used for neutral gels.^{144, 173, 174} The model equations containing L and ξ are discussed in **Paper I**, equations (2) and (5). Ξ is the correlation length that is related to the average distance between polymer-rich regions, and correspondingly L describes the correlation length between two adjacent cross-links inside these polymer clusters. Together, these two length scales form the overall structure as illustrated in **Figure 4.1**.

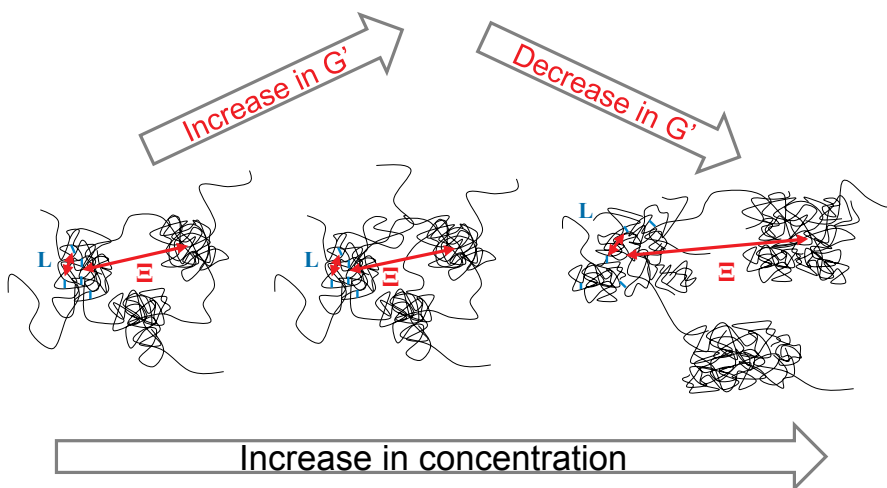


Figure 4.1. Structure of the gel with two length scales related to the storage modulus G' .

The correlation length L that describes the smaller sizes inside the polymer clusters is rather constant with polymer concentration and closely related to the persistence length of HA of 8 nm.¹⁷⁵ The distance between the polymer clusters, Ξ , is in the range of 1000 Å or larger for the two lower polymer concentrations (5 and 15 mg ml⁻¹), whereas for the highest concentration (30 mg ml⁻¹) this size is almost doubled. This distance is believed to affect the rheological, or viscoelastic properties of the gels, as the storage modulus for a gel depends on the macromolecular connectivity, in this case the link between the polymer-rich regions. The storage modulus G' increased eight-fold between the gels with concentrations of 5 and the 15 mg ml⁻¹, while dropping below the value for the gel with 5 mg ml⁻¹ when further increasing the concentration to 30 mg ml⁻¹. G' for the 5, 15 and 30 mg ml⁻¹ gel is 20, 160 and 2 Pa respectively. For the two lower gel concentrations Ξ is constant, and the increase in the storage modulus is explained by an increase in the number of links between the polymer clusters, forming a more stable gel structure. The explanation for the decrease of the storage modulus measured for the highest gel concentration is the increase in Ξ . This is caused by inadequate mixing. Previous studies have shown that different extents of mixing

during the gel preparation affects strongly the swelling behavior.¹⁷⁶ The swelling is directly related to the macromolecular connectivity inside the gel. The HA-A component, due to the high molecular mass, is much more viscous compared to the PVA-H component, especially at high concentrations. Mixing of a highly viscous component with a less viscous component during a gelation process would create a structure with many local cross-links that would increase the density of local networks without having any extensive connectivity between them. The suggested structure for the 30 mg ml⁻¹ gel that explains the lower modulus would thus consist of many dense clusters which are not well linked together. The gel structures with different polymer concentrations and their relations to the storage modulus G' are illustrated in **Figure 4.1**. The precise values of the storage moduli are listed in Table 3 in **Paper I**. This study highlights the inhomogeneous structure of two-component hydrogels as well as the requirements of proper mixing during preparation in order to achieve gels with full strength.

The 15 mg ml⁻¹ gels containing 5, 10 and 20% nanoHAP were measured with SANS where the gel matrices were contrast matched to the solvent. The shape of the scattering curves suggests that the particles consist of singly and aggregated nanoHAP, shown in **Figure 4.2**. The single particles could be modeled as disk-shaped cylinders with a radius of 100 ± 10 Å and the height of 30 ± 4 Å, with about 20% polydispersity for all measured contrasts. These dimensions are in agreement with previously reported transmission electron microscopy data.⁵⁵ The overall size of the particle aggregates could not be determined precisely due to the limited data range; however, the lower limits indicate a cluster size of about 1000 Å. The dimensions of the single particles are larger than the smaller correlation length L in the pure gel. The lower limit of the size of the aggregates is in the same range as the larger correlation length Ξ for the pure gel. This suggests either that the particles, singly or aggregated, are distributed around the cross-links and not only in the voids in between them, or that the particles perturb the local structure of the gel. Unfortunately, the particles contribute about 1000 times more to the total scattered intensity than the gel matrix alone; which makes it very difficult to match out the scattering from the particles to only observe the structure of the gel in a gel composite.

These gel composites showed a scattering pattern that could be superimposed by scaling by the concentration of nanoHAP. Previous studies with these hydrogel composites showed increased modulus and increased ectopic bone formation as the amount of particles increased.¹⁷⁷ This result demonstrates that the particle arrangement inside the gel matrix is concentration independent, despite the differences in the clinical outcome. In this case the amount of material has a big influence that cannot be ascribed to different structures of the material.

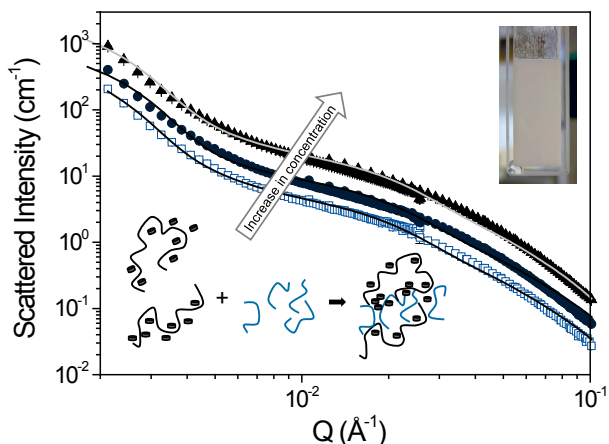


Figure 4.2. SANS for contrast matched gels with 5 (\square), 10 (\blacksquare), and 20% (\blacktriangle) nano-HAP.

4.2 Density profiles of grafted and adsorbed HA

Surface modifications of biomedical materials and devices by HA are one of the most attractive options in biomaterial coating strategies. HA does not only exhibit desirable physical properties (hydration, viscosity, space filling), it is as well biocompatible and bioactive.⁴ Information on the structure and conformation of surface-linked HA at an aqueous interface is extremely rare,⁴ which motivates the aim for this study. Neutron reflectivity measurements were performed on surface-grafted and surface-adsorbed HA polymers immersed in water. This technique provides information regarding the interfacial thickness, roughness and composition as discussed in chapter 3.3.1. The data analysis is described in chapter 3.3.2. A density or volume fraction profile of HA at an interface can be calculated from the scattering length density profile. The volume fraction profile of HA indicates the degree of hydration, the organization, and the quantity of the surface-linked HA at different distances from the surface. The volume fractions for different types of deposition protocols on various surfaces are shown in **Figure 4.3**, the inset shows an expanded part of the profiles for the first 150 Å from the surface.

As discussed in **Paper II**, HA-A was grafted onto an aminated silica surface where the modified aldehyde groups (6%)²⁶ on the HA backbones were covalently bound to the substrate. This procedure gives a stable structure which is not affected by rinsing. It can be concluded that due to the persistence length of the HA polymer (8 nm)¹⁷⁵, and the average distance between two aldehyde groups (17 nm), not all groups would react and an extended structure could be expected. The grafting was performed either by a single-

stage or a two-stage deposition. The single-stage deposition led to a less extended structure (dark blue line in **Figure 4.3**). The concentration used (10 mg ml^{-1}) was high and the deposition protocol allowed the attachment to occur in a single process, which led to a structure with a rather high initial volume fraction compared to the two-stage deposition. The two-stage deposition was performed using a 5 mg ml^{-1} solution which led to a lower volume fraction close to the surface (dark red line in **Figure 4.3**). The reaction with the polymer solution was, however, allowed to occur twice, resulting in a much more extended profile. An exponential function was used to fit these profiles. However, for the single-stage deposition of HA-A, a linear or a parabolic profile would fit the data as well (shown as the dotted blue line and light blue line respectively). For the two-stage deposition of HA-A, the linear or the parabolic profile does not give as good agreement with the experimental data as the exponential model (the dotted red and light red lines indicate the linear and a parabolic fit respectively).

Smooth varying density profiles are appropriate to describe polymers and gels at interfaces,¹⁶⁴ and the results from this experiment indicate that an exponential profile is suitable for both deposition protocols. The surface coverage is much higher for the sample prepared by a two-stage deposition ($2.2 \pm 0.5 \text{ mg m}^{-2}$). The value for the single-stage deposition is only about a third of that ($0.8 \pm 0.2 \text{ mg m}^{-2}$).

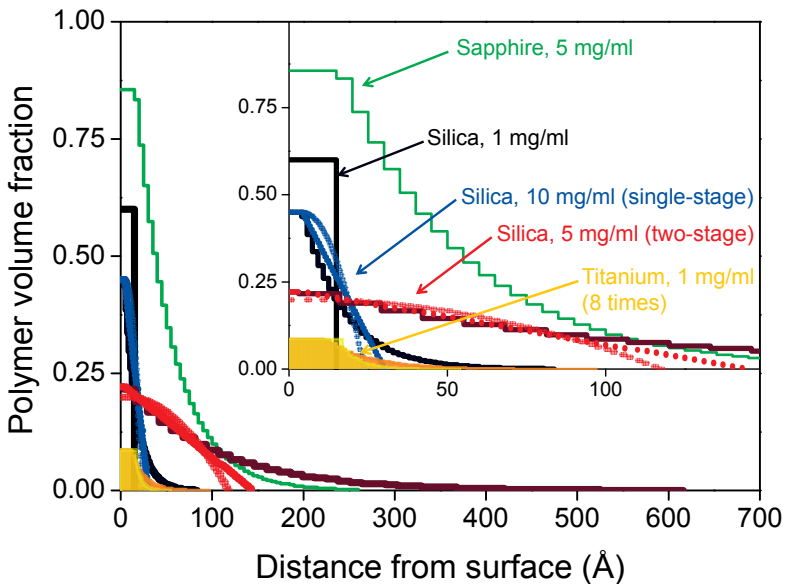


Figure 4.3. Polymer volume fraction profiles for grafted and adsorbed HA. No interfacial roughness is shown for clarity. The inset shows the first 150 \AA from the surface, with color-coded arrows that indicate the different HA grafting or adsorption procedures. All profiles on silica are for grafted HA, the rest indicate the in-situ adsorbed HA.

Carbodiimide-coupled native HA of 1 mg ml^{-1} on silica (black line in **Figure 4.3**), however, could be modeled without an extended profile. A model with a uniform layer had as good agreement with the experimental data. The layer was 15 \AA thick with 40% solvent penetration. This more compact structure is believed to be generated by the grafting chemistry. The EDC coupling enables all carboxyl groups of the HA repeating units to react with the surface-anchored primary amines, which produces a rigid and dense HA film on the surface. The surface coverage is similar to the HA-A sample prepared by a single-stage deposition ($0.9 \pm 0.2 \text{ mg m}^{-2}$).

These three examples of grafting HA on silica show that the structure and composition depend on the immobilization chemistry, the deposition protocol, and the concentration. Using a procedure based on a high HA concentration and a large number of surface-attachable points would create a structure that is denser close to the surface, which might possess good barrier properties. In contrast, a structure with a low initial polymer volume fraction but long decay profile could be achieved using multiple deposition steps and lower polymer concentrations. Such surface might be useful for the delivery of drugs or other small molecules. This information provides the possibility to tailor the desired surface property. One may choose other types of reaction mechanisms to immobilize the HA, increase the number of deposition steps and even vary the concentration or molecular mass for each step to obtain the preferred surface structure.

To verify the physical model for the grafted polymer layers, XPS and ellipsometry experiments were conducted to pre-characterize the interfaces as described in chapter 2.3.4. More details are found in the supplementary information for **Paper II**.

For the in-situ adsorption of HA, one could follow the process entirely with neutron reflectivity measurements. The in-situ adsorption of HA on both sapphire and TiO_2 was performed in two contrasts, D_2O and H_2O . The sapphire surface has the advantage of having a scattering length density ($5.75 \times 10^{-6} \text{ \AA}^{-2}$) close to D_2O ($6.35 \times 10^{-6} \text{ \AA}^{-2}$), e.g. far from that of the HA ($2.20 \times 10^{-6} \text{ \AA}^{-2}$). The large changes in the reflectivity in D_2O contrast for the substrate with adsorbed HA (green circles) compared to that of bare sapphire (black circles) are shown in **Figure 4.4**. The H_2O contrast gave only a minor visible change when plotting the RQ^4 as a function of Q , the grey squares indicate the bare surface and the purple squares the HA adsorption. The effect of the alteration of the surface by HA was, however, barely visible when plotting the log reflectivity as a function of Q .

The significance of the changes caused by HA adsorption is not entirely comparable to the visible difference in particular plots. A thin, hydrated layer of polymer with a long decay profile might not alter the curves in the same manner compared to a dense, thick, but uniform layer, even if both have identical Γ . Low contrast differences between the measured material

and the bulk solution also contribute to the difficulties in detecting the changes in reflectivity.

HA was deposited on titanium oxide surfaces by a layer-by-layer strategy. By alternating HA-A and HA-H (four times each), it is predicted that an HA gel would form on the surface as the two different HA components could cross-link. Even in D₂O contrast, the changes in reflectivity curve for the layer-by-layer adsorbed HA (green circles) compared to the one of bare TiO₂ (black circles) were very small; see (c) and (d) in **Figure 4.4**. A more obvious effect of the alteration of the surface by HA is observed when plotting the RQ^4 as a function of Q as compared to the logarithmic plot.

The difference in reflectivity data in D₂O contrast in the presence and absence of HA on sapphire (green arrow in (a) and (b) in **Figure 4.4**) is much larger compared to the one for the titanium oxide surfaces. The profiles for these two samples also show that the initial HA volume fraction on sapphire is several orders of magnitude higher and the overall thickness is almost three times higher. The overall surface coverage for HA adsorbed on sapphire is also much more substantial compared to the HA adsorbed on TiO₂ (4.7 mg m⁻² compared to 0.2 mg m⁻²). Both are fitted with an exponential profile.

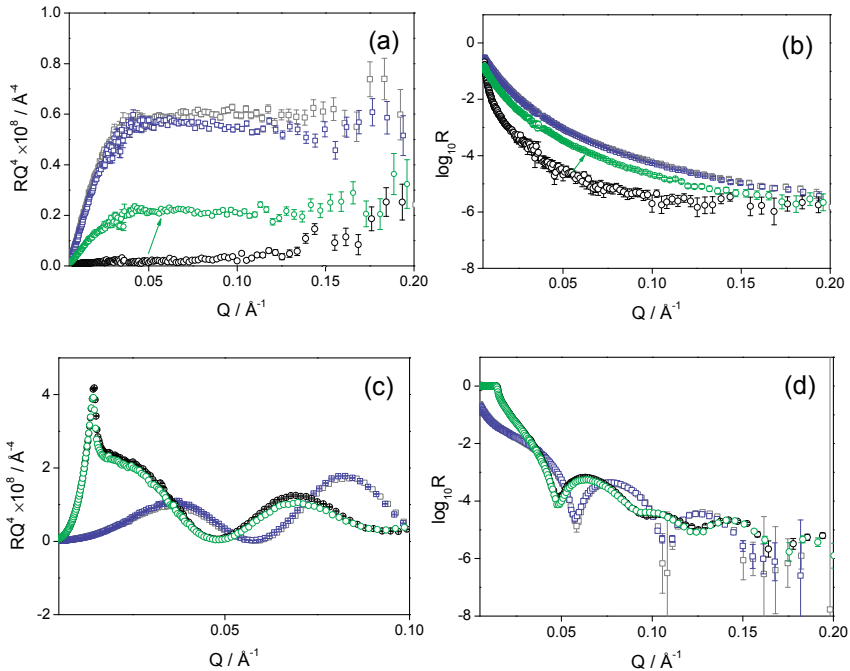


Figure 4.4. Neutron reflectivity data for HA adsorption on sapphire (a) and (b) and titanium oxide (c) and (d), shown as log reflectivity R as a function of Q , and $RQ^4 \times 10^8$ as function of Q . The bare surfaces are measured in D₂O (\circ) and H₂O (\square). The subsequent HA adsorption on both sapphire and TiO₂ are shown in green in D₂O and purple in H₂O.

The concentration and deposition method aside, it is expected that a thin and hydrated HA layer would be challenging to detect on the titanium oxide surface. This is due to the sputtered titanium and the titanium oxide surface with a thickness of about 120 Å and 30 Å respectively dominating the signal. The fringes created by the metal will make the changes caused by a thin polymer film to appear insignificant. The scattering length density of TiO₂ ($2.63 \times 10^{-6} \text{ Å}^{-2}$) is also very close to HA, which would further challenge the modeling of the data.

The parameters from the fit for the grafted and adsorbed HA are listed in **Table 4.1**. The 5 mg ml⁻¹ HA solution adsorbed on sapphire showed the largest initial polymer volume fraction as well as the highest overall surface coverage. The 8 times layer-by-layer deposition of the 1 mg ml⁻¹ HA-BP and HA on titanium oxide showed the smallest initial polymer volume fraction as well as the lowest surface coverage. Despite the large amount detected on sapphire, the stability of this HA structure is very sensitive to changes in pH. The experiments described in **Paper III** showed that the adsorbed HA layer at pH 3.9 could be completely removed by rinsing the surface with a solution of pH 7.4. Usually for long-term implants, a stable coating is needed which is often achieved by grafting of HA on a surface. However, an adsorbed layer does not necessarily indicate bad durability. HA with BP groups have very strong attachment to titanium oxide through Ti-O-P bonds. HA without the BP groups have also stronger attachments to TiO₂ compared to the native HA adsorbed on sapphire. It is, however, easier to draw conclusions about the interaction between a firmly grafted layer with other molecules or ions if one can assume a constant amount of HA.

Table 4.1. The parameters for the grafted and adsorbed HA on various surfaces.

Sample	Polymer concentration (mg ml ⁻¹)	<i>t</i> (Å)	φ _w (%)	<i>l</i> (Å)	Γ (mg m ⁻²)
Silica single-stage grafted HA-A	10	4±2	55±8	13±2	0.8±0.2
Silica two-stage grafted HA-A	5	3±3	78±2	100±20	2.2±0.5
Silica EDC grafted HA	1	15±5	40±15	--	0.9±0.2
Sapphire adsorbed HA	5	15±3	15±3	40±10	4.7±0.7
Titanium oxide adsorbed HA-BP	1	18±4	91±10	6±2	0.2±0.05
Titanium oxide adsorbed HA	1	11±3	91±10	14±4	0.2±0.05

4.3 Interactions of HA with ions and proteins

The structure of grafted HA could be altered by many different factors, such as changes in the ionic strength of the solvent or by interactions with other molecules. During the course of one experiment (a duration of a few days), as long as the grafted layer is well-prepared and extensively rinsed, it is as-

sumed that the amount of material on the surface is constant. HA is usually degraded by enzymes. However, it can also be degraded by non-enzymatic means such as acidic or alkaline conditions, physical stress, sonication, or free-radical based cleavage.¹⁰ Ellipsometry measurements of the samples before and after a neutron reflectivity study show that the samples are essentially unaffected. The interaction of ions on grafted HA was studied with neutron reflectivity, discussed in **Paper II**. The protein interaction was studied by two techniques: SANS was used for the HSA and HA co-adsorption to latex particles and neutron reflectivity measurements were made for the HSA and BMP-2 adsorption to surface-tethered HA. The HSA interactions with HA are discussed in **Paper III** and the BMP-2 interactions with HA are presented in **Paper IV**.

The solvent surrounding the grafted HA-A was changed from containing monovalent sodium ions to divalent calcium ions, described in **Paper II**. Being an anionic polymer, the structure of HA was influenced by the increase in valency of cations in solution. Measurements of solutions of HA have shown a decrease in the radius of gyration when calcium ions were introduced.⁴⁷ This conformational change may offer a mechanism by which cells can facilitate movement through the extracellular matrix by secreting small amounts of ions.⁴⁷ In the neutron reflectivity measurements, the change of solvent influenced the single-stage and two-stage grafted HA-A in a similar fashion. An increase in the initial polymer volume fraction as well as a decrease in the extended profile was observed, e.g. an overall compression of the structure. Although due to the denser packing of the HA-A deposited in a single-stage, a more concentrated solution of calcium ions was needed to alter the structure. The compressive effect was not as pronounced as for the HA-A deposited in two stages. The polymer volume fraction before and after calcium interactions for both samples are shown in Figure 7 in **Paper II**. Calcium ions can bridge between two anionic polymer chains, acting as a cross-linker. A polymer structure that is more diffuse and that has a more extended conformation is more sensitive to the penetration of these counter-ions. The structures after the ionic interaction were also able to withstand further rinsing of pure solvent, maintaining the collapsed state of the polymer layers.

In **Paper III**, the interaction of HA with HSA on latex particles and on silica substrates was compared. These surfaces differ in size, hydrophilicity and charge. They can be considered as mimics for some of the biomaterial surfaces that are used currently.^{56, 178, 179} SANS measurements was performed to study the adsorption and co-adsorption on the nano-sized latex particles. HSA adsorption on latex alone was studied to provide a reference for the investigation of the co-adsorption of mixtures of HSA and HA solution. HSA molecules form a shell around the latex core. The shell thickness increases linearly with added bulk concentration for concentrations less than 5 mg ml⁻¹. The fraction of unbound HSA that remained in solution also in-

creases with concentration. The parameters of the fits and the calculated surface coverage are listed in **Table 4.2**. Different orientations of the HSA molecules based on the shell thickness have been proposed by Song and Forciniti.¹⁸⁰ The adsorption isotherm is shown in **Figure 4.5**, together with the possible HSA orientations illustrated as inspired by the work of Song and Forciniti.¹⁸⁰

Table 4.2. Results from analysis of SANS data for HSA coated latex at pH 4.8.

Concentration (mg ml ⁻¹)	Shell thickness (Å)	Surface coverage (mg m ⁻²)	% HSA that is unbound	HSA molecules per particle
1.2	32±2	0.7±0.1	23±5	106
1.6	44±2	1.5±0.2	21±3	214
2.0	52±2	1.7±0.2	34±3	240
3.2	86±4	2.1±0.3	38±2	300
5.0	105±4	2.3±0.3	52±3	333

Adsorption of a protein by hydrophobic association is at its maximum at pH = pI for the adsorbate,¹⁸¹ in this case pH = 4.8. At this pH, the adsorbate has the minimum solubility in the bulk and the lowest repulsion in the interfacial layer.¹⁸² Adsorbing HSA on bare latex at the pI of HSA shows an adsorption isotherm behavior with a plateau that was not reached in the concentration range studied, as shown in **Figure 4.5**.

HA is anionic at pH>3.⁶⁹ At a pH between 3 and 4.8, the electrostatic interactions between the positively charged HSA and the negatively charged HA could mediate the binding of HA to latex through HSA. At a pH of 3.9, the HSA and HA was observed to co-adsorb on latex, as indicated by the scattering data shown in **Figure 4.6**. The difference between the latex with HSA alone compared to the latex with co-adsorbed HSA and HA is clear. Although the difference is small, it is similar to that seen when the absorbed amount of HSA increases. The data can still be fitted adequately with a core-shell model but it is difficult to distinguish the HSA and HA composition in the shell because of the small differences in ρ for the two molecules. The highest HSA mediated adsorption of HA was observed for HA of molecular mass lower than 150 kDa at concentrations above 2 mg ml⁻¹. HA of molecular mass over 1 MDa caused the samples to flocculate. This suggests that very long chains of HA can form bridges when adsorbed between different particles leading to precipitation. In general, lower concentrations of protein alone (<1 mg ml⁻¹) or low concentrations of HA in the mixture with HSA can also cause sample flocculation. This is due to the destabilization of the system that occurs by neutralizing the small repulsive charges between particles which flocculates the dispersion. Higher concentrations, however, led to a full coverage and stabilized the system as coated particles.

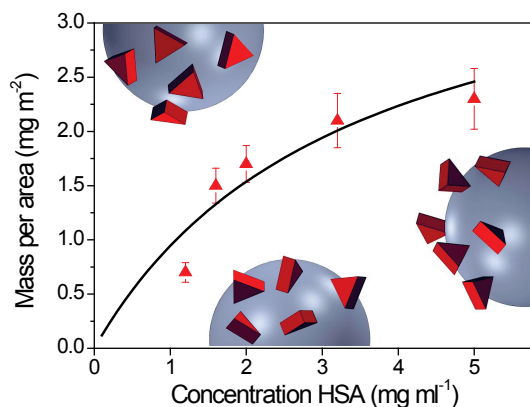


Figure 4.5. Adsorption isotherm for HSA on latex at pH 4.8. The insets illustrate the possible orientations of HSA on the latex particle surface.

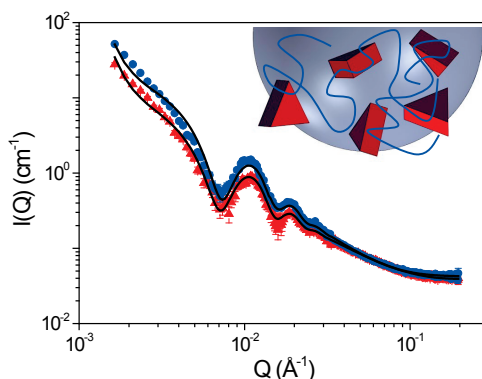


Figure 4.6. SANS data for the adsorption on latex particles that are contrast matched with the solvent. The adsorption of HSA alone (▲) is compared with the HSA and HA co-adsorption (●). The inset illustrates the HSA as red triangles and HA as blue strands.

The electrostatic interactions between HSA and surface-tethered HA were studied using neutron reflectivity. HA was covalently linked to a silica substrate using a carbodiimide-mediated condensation. As mentioned previously, grafting of HA is a more suitable procedure for long-term surface modifications. It gives a stable structure that can withstand rinsing and is a good reference substrate as the polymer surface excess is not altered by the protein interaction. Figure 8 in **Paper III** summarizes the molecular density profiles for the grafted HA layer and the change that occurs after adsorption of HSA at pH 4.8. The thin, grafted HA layer was observed to be unchanged before and after the HSA interaction. Once the protein was introduced, it was possible to model the reflectivity data as a diffuse layer of HSA on top of the originally grafted HA layer. The adsorption of HSA did not create a uniform layer but rather formed an extended density profile similar to that of loosely bound polymers. The overall thickness was more than 400 Å. This protein

adsorption was, however, reversible. Increasing the pH of the solution to 7.4 removes all the protein bound to HA leaving the scattering data identical to that of the originally grafted HA layer. The HSA surface coverage was $9 \pm 1 \text{ mg m}^{-2}$. This value is much higher than Γ for the HSA adsorbed on bare latex ($0.7 \pm 0.1 \text{ mg m}^{-2}$). This suggests that the ionic interaction is much stronger than the hydrophobic adsorption mechanism.

Titanium oxide surfaces prepared by sputtering metallic titanium onto silicon substrates were used for studies described in **Paper IV**. These surfaces can mimic the surfaces used in orthopedic inserts. The interaction of BMP-2 with HA gel coated TiO_2 was compared to the bare titanium oxide surface. Despite the small amount of HA on titanium oxide, this thin layer was sufficient to modify the surface and change its susceptibility to bind BMP-2. One of the coated HA gels contained additional BP groups. These groups can anchor to the metal oxide surfaces through Ti-O-P bonds. The layer was, as expected, a little bit thicker with a less extended profile compared to the HA polymer without BP groups. The HA-BP coated layer, the HA layer and the bare metal oxide surface and their interactions with BMP-2 were measured using QCM and neutron reflectometry. The results are described in detail in **Paper IV**. The neutron reflection data are presented in the supplementary information and the calculated volume fraction found after each injection step is shown in Figure 6 of that paper.

The QCM data for the HA-BP coated titanium oxide and the subsequent BMP-2 interactions are shown in **Figure 4.7**, where the curves in different shades of blue indicate the changes in the normalized frequency for the different overtones 3, 5, 7, 9 and 11 (the darkest shade is for the lowest overtone number). The QCM follows the polymer and protein adsorption, as well as the rinsing processes. The drop in the normalized frequency ($\Delta f / n$) indicates an increase in mass on the QCM sensor. The first injection of the polymer was sufficient to cover the sensor surface and, interestingly, no further binding was detected after that layer was formed. Only small shifts were observed for the different overtones after rinsing away the unbound material, which indicate that the polymer film left on the sensor is relatively rigid. This could be fitted to a thickness of about 30 Å using the Sauerbrey relations.^{113, 114} After the injection and the rinsing of BMP-2, the Sauerbrey relations are no longer valid as the differences of the overtones are larger, indicating a more viscous layer. The large decreases in $\Delta f / n$, however, show that a substantial amount of BMP-2 has been adsorbed even for the dilute ($7.5 \mu\text{g ml}^{-1}$) solution. Rinsing with calcium chloride increased the normalized frequency and after further rinsing with pure water, the data returned roughly to the level of that of the bare HA-BP coating, indicating that all the adsorbed BMP-2 had been desorbed.

The QCM data for the HA gel coating (without the BP groups) showed similar polymer adsorption but with higher amounts of BMP-2. However, the two rinsing steps with calcium chloride and water could only remove a

small fraction of the total absorbed amount. Calcium had no significant interaction with the BMP-2 adsorbed on the bare (non-polymer coated) metal oxide surface. These results are shown in Figure 2 in **Paper IV**.

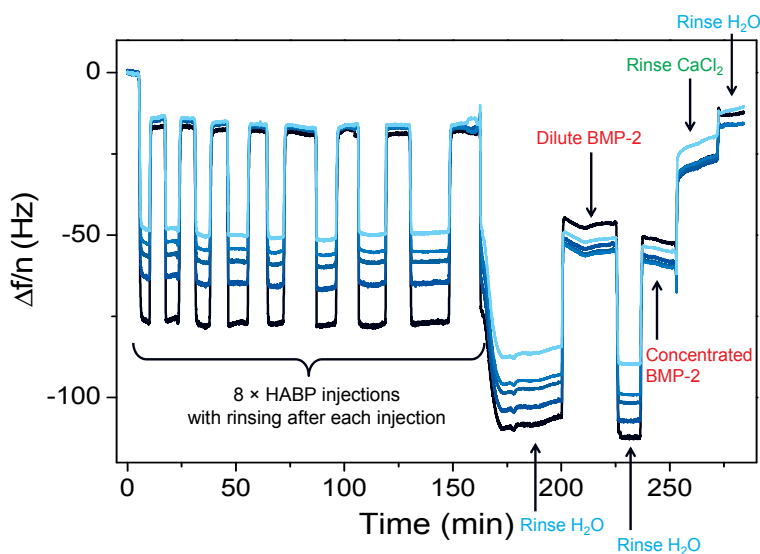


Figure 4.7. QCM data for the normalized frequency change as a function of time during each of the deposition steps. HA-BP-H alternated with HA-A (injected 8 times in total with rinse between each step) followed by injection of BMP-2 (dilute and concentrated solutions), and rinsing with CaCl₂ and H₂O.

Neutron reflectivity data confirmed the results from the QCM data and, in addition, it provided more information regarding the structure and composition. The HA-BP layer and the HA layer have the same surface coverage, but due to the slightly more extended structure of the HA lacking the BP groups, more adsorption of protein was observed. This confirms the conclusion from section 4.2, where the importance of the structure, and not only the amount of polymer on the surface, is believed to be crucial for the surface properties.

The BMP-2 layers on both gel coated surfaces and the bare titanium oxide surface showed a profile containing a low protein density region, followed by a higher density region with a decay profile (Figure 6 in **Paper IV**). It is believed that this density profile is caused by the non-uniform shape of the BMP-2 molecules, which makes it difficult for the molecule to be packed in a well-organized manner. Increasing the BMP-2 concentration from 7.5 to 37.5 $\mu\text{g ml}^{-1}$ increased the protein surface coverage for the gel coated surfaces but not for the bare titanium oxide surface.

The desorption properties of BMP-2 on the HA-BP gel are much more pronounced compared to that from the HA gel that lacks BP groups. In the same manner as observed in the QCM measurements, the dissolved calcium ions did not alter the profile of the BMP-2 layer on the bare TiO₂ significant-

ly. **Table 4.3** lists all the BMP-2 surface coverages before and after the interactions with calcium. It is documented that HA-BP has very strong interactions with calcium ions.³⁰ These ions could efficiently replace a substantial amount of the BMP-2 bound to HA-BP, releasing the protein to the bulk solvent. This calcium triggered release of BMP-2 from the HA-BP coated material could provide a surface with tunable growth factor delivery properties. This process is crucial for the activation of bone regeneration. This study has highlighted the bioactivity of HA as a coating material.

Table 4.3. The surface coverage Γ (in mg m^{-2}) of BMP-2 for samples before and after rinsing with calcium chloride.

Sample	Dilute BMP-2	Concentrated BMP-2	Rinsing with calcium
HA-BP coating	2.0±0.3	3.0±0.5	1.4±0.3
HA coating	3.3±0.4	4.9±0.5	4.5±0.4
Bare TiO ₂	4.4±0.4	4.4±0.5	4.0±0.5

5 Concluding remarks and future perspectives

The structure of HA in the bulk and at interfaces is related to the physical properties of biomaterials as it determines the mechanical performance and surface interactions, as well as mechanisms for delivery of therapeutic agents. Information about the nanostructure for an applicable medical device material guides the formulation, preparation, and use. In turn, this should lead to further understanding of its exploitation.

HA hydrogels are inhomogeneous in structure and the rheological properties depend on the polymer concentration. Although it is possible to increase the stability of a hydrogel matrix by adding a reinforcing material, one should keep in mind the importance of adequate mixing during the preparation to achieve full gel strength. The structural arrangements of particles in a gel composite was observed to be independent of particle concentration, although higher amounts are still favorable to promote bone regrowth as one introduces more building blocks to a wounded bone fracture site.

Solvated HA grafted on a surface could best be described with a density profile that decays exponentially towards the bulk solution. This distribution depends on the deposition protocol, the concentration, and the number of possible attachment points between the HA and the substrate. A more compact structure can be created using a single-stage deposition protocol, a more concentrated HA solution and an immobilization chemistry that contributes to more reactive sites with the surface. These types of surfaces are believed to possess good barrier properties, for example as coatings to increase lubrication to the surrounding tissue.

In contrast, a structure with a low initial polymer volume fraction and a long decay profile could be achieved using multiple deposition steps and lower polymer concentrations, as well as fewer possible attachment points. More extended structures were found to be more responsive to external stimuli such as changes of counter-ions. More extended structures can also adsorb a higher amount of protein. A structure with a lower density profile may have useful properties for the delivery of small molecules, for example drugs or proteins. Information linking the density profile with the deposition protocol provides the possibility to tailor the desired surface property.

For long-lasting polymer films, a well-grafted HA layer is required. The interaction of HA with a protein is not straightforward to predict. Both electrostatic interactions and chemical reactions account for the protein adsorption and desorption on top of surface-tethered HA.

In summary, the structure of HA hydrogels and the density distribution of HA at solid-liquid interfaces were studied, providing a first characterization of a relatively complex system. Neutron scattering was successfully applied to investigate the hydrated structure of HA, as well as its interactions with other biomolecules. This study would have benefited from work with deuterated HA as it offers additional contrasts in the study of complex, multiple-component systems. Deuterated HA could be cultured using a bacterial strain (*Streptococcus zooepidemicus*) in deuterated media (d_7 -D-glucose, D_2O). However, the purification and characterization still remain to be optimized before being able to use this molecule in a scattering experiment.

6 Acknowledgements

And it is done! Four years have passed, four years filled with experiences no money in the world can buy.

Jag vill börja med att tacka professor *Jöns Hilborn* för möjligheten att jobba inom ett helt nytt och spännande projekt, och för att ha gett mig så mycket frihet under mitt arbete.

Professor *Adrian Rennie*, thank you for your patience, for all your help and for sharing your knowledge. I really appreciate that you flew to France for all my beamtimes and for the work on my papers and thesis. You are an incredible scientist and an inspiration! Thank you for everything!

Giovanna Fragneto, thank you for all your support during my stay in Grenoble. You are as they call you, the queen of reflectivity.

Yuri, co-author, colleague and comrade. Thank you for being my go-to-guy for everything imaginable. I have learned a lot from you, from fitting with Origin to what mushrooms one can eat, and of course, the latest workplace gossip. And most of all, thank you for being such a good friend!

Thank you *Lionel*, for the times spend on D22. Thank you *Dmitri*, for getting interested in neutron reflectivity and for all the materials you provided. *Maja*, tack för att du delar med dig av din erfarenhet, vare sig det handlar om neutroner eller Prop eller om livet mellan Grenoble och Uppsala.

Isabelle Morfin, thank you for our discussions about protein/HA interactions. Thank you professor *Marguerite Rinaudo* for the guidance in the CERMAV lab, for teaching me about HA purification, and for the useful discussions during the writing of my first paper. Thanks to the people in the LSS group for keeping the instruments and programs running, and for always taking the time to answer my questions. And I am really grateful to so many of you at the ILL for helping me deal with the French bureaucracy.

Thanks to the colleagues in the polymer group; *Tim*, *Kristoffer*, *Oommen*, *OP*, for the help in chemistry, biomaterials and for your enthusiasm about gels. Tack *Cissi*, *Sonya*, *Jonas* och *Gry* för gott sällskap under min tid på Ångström. Tack *Sonya* för poster- och cover lettermallarna och din powerpoint expertis. Tack *Jonas* för korrekturläsningen och avhandling- och manuskriptmallarna. *Youka*, thanks for the past few months in the office. You, together with the others that regularly visit our office, have unintentionally been teaching and improving my Chinese. And to the rest of the PhD students in the group, *Sujit*, *Yu*, *Uzma*, *Hongji* and *Shujiang*, enjoy the rest of your time here. *Janne*, tack för att du delar mitt intresse till musiken.

Tack *Tatti* för att vara kontorsmamma och ser till att jag skriver på allt som så lätt glöms bort. Ett stort tack igen till *Kristoffer*, *Cissi*, *Sonya*, *Jonas* och *Maja*, vars avhandlingar jag har bläddrat sönder och samman. Tack resten av materialkemin för fiket och andra trevligheter. Tack *Erik* and *Matilda* för sputtringen och tack *Peter* som ser till att min dator funkar som det ska.

To the materials physicists across the corridor, thanks for accepting me as one of you and for good company! *Gunnar*, tack för att du lärde mig allt om reflektivitet. *Andreas* för designen av provhållaren till sputter. *Anna*, thanks for sharing my experience and knowing exactly what I am going through.

Tack *Jim* och *Inger* för er hjälp med hyareningen och karakteriseringen.

Thanks to *Peggy*, for all our coffee breaks where no coffee was consumed, and our trips and our heart-to-heart. I really appreciate our friendship. *Joni* and *Andrew*, for being annoyingly entertaining, and for being there when times get rough. You guys rock! *Alexis*, for making all the administrative phone calls and for at least trying to force me to speak French. *Ingo*, *Anton*, *Andrew D*, *Manu*, the post docs that are always up for a beer or two, and for always having the funniest “scientific” theories about everything. The Italian mob: *Yuri*, *Federica*, *Francesco*, *Giacomo*, *Ernesto* etc, thank you for filling our office with laughter and Italian. *Eva*, *Eron*, *Diana*, *Louis*, keep up the traditions and don’t let the obscure lunch discussions die out! *Christian*, *Mario*, *Rita*, and *Simone*, thanks for sharing my interest in climbing. To all the people I got to know during my time in Grenoble, thanks for all the fun times we shared, the parties, dinners, barbecues, crêpe-evenings, squash games, ski trips, hikes, and travels! You guys made my Grenoble experience unforgettable and one of the greatest times of my life!

Tjejerna *Anna*, *Hanna*, *Jessi* och *Matilda*, jag är så glad att jag har er! Tack för att ni finns där för mig oavsett hur långt borta jag befinner mig. Ni betyder fruktansvärt mycket för mig! *Karin*, tack för din vänskap och din soffa. *Anna G*, för att du visar mig en värld utanför jobbet och för vårt äventyr i Rivieran. *Henrik*, för glassen som borde ha erbjudits flera år sedan, och att du ska bli min toast. Tack till gamla kursare, nationskörerna och spexen för studentlivet i Uppsala!

And thanks all of you that I may have forgotten to mention.

I am grateful to my family, thank you *mom* for pushing me, and always made me believe that I can do anything. Thank you *grandma* and *grandpa* for setting the bar so high and being supportive all the way. Tack *pappa* för att du skjutsar och lämnar och fixar allt smått. And thank you *Tiantian* and *Nan*, for keeping my parents company when I’m in France and for being my private IT support. Thanks *Nannan* for being there for our grandparents.

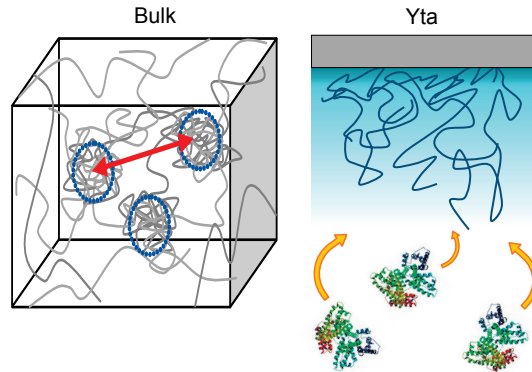
And finally, *Martin*, thank you for these three wonderful years we spent together and for all the fun we had. Thanks for giving me a home, for challenging me and for being my biggest support. Thank you for not only taking care of me but also my bikes and skis. And thank you for your big big heart. I mog di! I love you! Jag älskar dig!

7 Svensk sammanfattning

Hyaluronan upptäcktes av Karl Meyer under 1930-talet i ögats glaskropp. Denna slemmiga, långa sockermolekyl väckte snabbt intresse inom många vetenskapliga discipliner. I den extracellulära matrixen (omgivningen utanför cellen som består av ett nätverk av stora molekyler) har den flera funktioner bland annat vid sårhäkning, cellvandring, inflammation med mera. Hyaluronan har också många fascinerande fysikaliska och kemiska egenskaper; den har en kraftig vattenupptagande förmåga, är stötdämpande och den är viskoelastisk (det vill säga har egenskaper av både fasta och flytande material). På senare tid har hyaluronan använts flitigt som biomaterial vid återbildning av vävnad, läkemedelstransport och som ersättare för ledväskor. Dock är den mest känd för allmänheten som fyllnadsmedel vid skönhetsbehandlingar och som tillsats i kosmetika.

I denna avhandling har hyaluronans nanostruktur undersökts. Syftet är att få en bättre förståelse för materialet när det används kliniskt. Hyaluronan kan tvärbindas för att forma en gel. Denna gel kan användas till att leverera partiklar och tillväxtfaktorer till kroppen. Hyaluronan kan också fästas på ytor av implantat så att ytan modifieras till att ha specifika egenskaper anpassade för medicinska ändamål. Dessa egenskaper kan vara att öka möjligheten för implantatet att fästa på kroppsegen vävnad, öka acceptansen för implantatytan i kroppen eller vara bioaktiva, det vill säga leda till reaktion i kroppen, till exempel öka läkningen. Både bulkstrukturen och ytstrukturen har studerats, detta illustreras i **Figur 7.1**. I studien har även ett antal olika fysiologiska miljöer simulerats som materialet kan tänkas utsättas för i kroppen. Hyaluronans struktur har bland annat studerats på ytor i lösningar med olika jonhalt, samt i kontakt med olika proteiner.

Resultaten i den här avhandlingen bygger i stort på mätningar med neutronspredningstekniker. Materialet placeras då i en neutronstråle som genereras av klyvning av uran i en kärnreaktor. Neutronerna interagerar med materialet, sprids och bildar ett spridningsmönster som kan tolkas om till materialets struktur. Eftersom neutronerna är oladdade så har de endast svaga interaktioner med materialet. Materialet förstörs inte heller av neutronerna i processen. Neutronerna ger oss en möjlighet att se strukturer djupt inne i material och komma åt dolda ytor.



Figur 7.1. Illustration av en bulkgel (till vänster) och hyaluronan på ytor (till höger). De gråa linjerna symboliserar polymerkedjorna som har tvärbundits till en gel. Bulkgelens struktur består av polymerrika klumpar av små tvärbundna nätverk. Ytbunden hyaluronan (blåa linjerna) har en densitetsprofil där densiteten avtar ju längre bort från ytan man kommer. Proteinerna långst ner till höger kan binda till hyaluronan.

Geler formade av tvärbunden hyaluronan visar upp oregelbundna (inhomogena) strukturer. Strukturen beskrivs med två olika långa tvärbindningsavstånd. Dessa avstånd beskriver porstorleken eller avståndet mellan två polymerkedjor. Ett av dessa avstånd kan relateras till gelens viskoelastiska egenskaper, som beskriver fastheten för en gel. Studien visar att gelens fasthet inte är proportionell mot ökad polymerkoncentration. För höga koncentrationer kan på grund av dålig blandning av komponenterna ge en gel med sämre kvalitet. Gelens stabilitet kan ökas genom att tillsätta keramiska nanopartiklar. När dessa partiklar är inuti gelen kan de både vara åtskiljda eller aggregera och forma klumpar med en radie större än 100 nm. Studien visar även att strukturen på partiklarna inte påverkas av partikelkoncentrationen, dock ger en högre koncentration bättre läkning vid benbrott då partiklarna tillförer det skadade benet med mer mineraler i form av dessa keramiska nanopartiklar.

Studier av hyaluronan fäst på ytor och studerad i vattenlösningar är väldigt ovanliga. Neutronreflektivitet är en teknik som studerar strukturer vid ett gränsskikt, till exempel mellan en fast fas och en flytande fas. Detta ger resultat i form av en densitetsprofil, där förändring av hyaluronans densitet i förhållande till avståndet från ytan beskrivs. För en hållbar yta måste hyaluronan fästas ordentligt, detta görs genom att kemiskt tvärbinda polymererna på ytan. Olika fästningsmetoder ger upphov till hyaluronan med olika egenskaper, det vill säga olika tjocklek, vattenhalt och utsträckning. Hur lätt hyaluronan som är fäst vid ytor påverkas av andra faktorer beror på strukturen. Är strukturen lös och innehåller mycket vatten kan ändring från natriumjoner till kalciumjoner få strukturen att kollapsa. Båda dessa joner

finns naturligt i kroppen. Skelettet består däremot av kalciummineraler. Långa lösa strukturer kan också binda mer protein.

I en annan studie har adsorption av hyaluronan och humant serumalbumin på hydrofoba latexpartiklar undersökts. Adsorption är ett ytfenomen som innebär att ett ämne fastnar på av ytan av ett annat ämne. Denna studie ger en modell för ytförändringar av kolloida partiklar för användning inom läkemedelstransport. Studien visar att adsorption av hyaluronan med hjälp av albumin är beroende av hyaluronans molekylvikt, pH samt molekylernas koncentration. Adsorption av albumin på ytbunden hyaluronan beror också på pH.

I den sista studien har adsorption och frisättning av BMP-2 på titanytor undersöks. BMP-2 är ett benmorfogenetiskt protein, en tillväxtfaktor som ökar kroppens benproduktion. Kemiskt modifierad hyaluronan på titanytan kan ge en kontrollerad adsorption av BMP-2. Protein som är bundet till hyaluronan kan sedan frisättas genom att ytan kommer i kontakt med kalciumjoner. Dessa joner binds till den modifierade hyaluronan istället för BMP-2 som då frisätts. De frisatta BMP-2 stimulerar kroppen att bilda ben.

Denna avhandling visar hur neutronspridningstekniker kan tillämpas för att studera strukturen på mjuka material, samt exempel på hur hyaluronan i framtiden kan användas kliniskt inom sjukvården för att till exempel påskynda läkning av benbrott.

8 References

1. Van Regenmortel, M. H. V., Analysing structure-function relationships with biosensors. *Cellular and Molecular Life Sciences* **2001**, 58, (5-6), 794-800.
2. Chen, W. Y. J., *Hyaluronan*. Woodhead Publishing Ltd.: Cambridge, U.K., 2002.
3. Chen, W. Y. J.; Abatangelo, G., Functions of hyaluronan in wound repair. *Wound Repair and Regeneration* **1999**, 7, (2), 79-89.
4. Morra, M., Engineering of biomaterials surfaces by hyaluronan. *Biomacromolecules* **2005**, 6, (3), 1205-1223.
5. Angelova, N.; Hunkeler, D., Rationalizing the design of polymeric biomaterials. *Trends in Biotechnology* **1999**, 17, (10), 409-421.
6. Lee, J. H.; Lee, H. B.; Andrade, J. D., Blood compatibility of polyethylene oxide surfaces. *Progress in Polymer Science* **1995**, 20, (6), 1043-1079.
7. Cohen Stuart, M. A.; Huck, W. T. S.; Genzer, J.; Muller, M.; Ober, C.; Stamm, M.; Sukhorukov, G. B.; Szleifer, I.; Tsukruk, V. V.; Urban, M.; Winnik, F.; Zauscher, S.; Luzinov, I.; Minko, S., Emerging applications of stimuli-responsive polymer materials. *Nat Mater* **2010**, 9, (2), 101-113.
8. Meyer, K.; Palmer, J. W., The polysaccharide of the vitreous humor. *Journal of Biological Chemistry* **1934**, 107, (3), 629-634.
9. Laurent, T. C.; Fraser, J. R. E., Hyaluronan. *Faseb Journal* **1992**, 2397-2404.
10. Capila, I.; Sasisekharan, R., *Chemistry and Biology of Hyaluronan*. Elsevier: Oxford, 2004.
11. Weigel, P. H., *Chemistry and Biology of Hyaluronan*. Elsevier: Oxford, 2004.
12. Sugahara, K.; Schwartz, N.; Dorfman, A., Biosynthesis of hyaluronic-acid by streptococcus. *Journal of Biological Chemistry* **1979**, 6252-6261.
13. Fraser, J. R. E.; Laurent, T. C.; Laurent, U. B. G., Hyaluronan: Its nature, distribution, functions and turnover. *Journal of Internal Medicine* **1997**, 242, (1), 27-33.
14. Matteini, P.; Dei, L.; Carretti, E.; Volp, N.; Goti, A.; Pini, R., Structural Behavior of Highly Concentrated Hyaluronan. *Biomacromolecules* **2009**, 10, (6), 1516-1522.
15. Lapčík, L. J.; Lapčík, L.; De Smedt, S.; Demeester, J.; Chabreček, P., Hyaluronan: Preparation, structure, properties, and applications. *Chemical Reviews* **1998**, 98, (8), 2663-2684.
16. Day, A. J.; Sheehan, J. K., Hyaluronan: polysaccharide chaos to protein organisation. *Current Opinion in Structural Biology* **2001**, 11, (5), 617-622.
17. Cowman, M. K.; Matsuoka, S., Experimental approaches to hyaluronan structure. *Carbohydrate Research* **2005**, 340, (5), 791-809.
18. Yokoi, N.; Komuro, A.; Nishida, K.; Kinoshita, S., Effectiveness of hyaluronan on corneal epithelial barrier function in dry eye. *British Journal of Ophthalmology* **1997**, 81, (7), 533-536.

19. Guillaumie, F.; Furrer, P.; Felt-Baeyens, O.; Fuhendorff, B. L.; Nymand, S.; Westh, P.; Gurny, R.; Schwach-Abdellaoui, K., Comparative studies of various hyaluronic acids produced by microbial fermentation for potential topical ophthalmic applications. *Journal of Biomedical Materials Research Part A* **2010**, 92A, (4), 1421-1430.
20. Karlsson, J.; Sjögren, L. S.; Lohmander, L. S., Comparison of two hyaluronan drugs and placebo in patients with knee osteoarthritis. A controlled, randomized, double-blind, parallel-design multicentre study. *Rheumatology* **2002**, 41, (11), 1240-1248.
21. Marshall, K. W., Intra-articular hyaluronan therapy. *Current Opinion in Rheumatology* **2000**, 12, (5), 468-474.
22. Stern, R.; Asari, A. A.; Sugahara, K. N., Hyaluronan fragments: An information-rich system. *European Journal of Cell Biology* **2006**, 85, (8), 699-715.
23. Patterson, J.; Siew, R.; Herring, S. W.; Lin, A. S. P.; Guldberg, R.; Stayton, P. S., Hyaluronic acid hydrogels with controlled degradation properties for oriented bone regeneration. *Biomaterials* **2010**, 31, (26), 6772-6781.
24. Leach, J. B.; Bivens, K. A.; Collins, C. N.; Schmidt, C. E., Development of photocrosslinkable hyaluronic acid-polyethylene glycol-peptide composite hydrogels for soft tissue engineering. *Journal of Biomedical Materials Research Part A* **2004**, 70A, (1), 74-82.
25. Shu, X. Z.; Liu, Y. C.; Luo, Y.; Roberts, M. C.; Prestwich, G. D., Disulfide cross-linked hyaluronan hydrogels. *Biomacromolecules* **2002**, 3, (6), 1304-1311.
26. Bergman, K.; Engstrand, T.; Hilborn, J.; Ossipov, D.; Piskounova, S.; Bowden, T., Injectable cell-free template for bone-tissue formation. *Journal of Biomedical Materials Research Part a* **2009**, 91, 1111-1118.
27. Bergman, K.; Elvingson, C.; Hilborn, J.; Svensk, G.; Bowden, T., Hyaluronic acid derivatives prepared in aqueous media by triazine-activated amidation. *Biomacromolecules* **2007**, 8, 2190-2195.
28. Ossipov, D.; Hilborn, J., Poly(vinyl alcohol)-based hydrogels formed by "click chemistry". *Macromolecules* **2006**, 39, (5), 1709-1718.
29. Ossipov, D.; Brannvall, K.; Forsberg-Nilsson, K.; Hilborn, J., Formation of the first injectable poly(vinyl alcohol) hydrogel by mixing of functional PVA precursors. *Journal of Applied Polymer Science* **2007**, 106, 60-70.
30. Yang, X.; Akhtar, S.; Rubino, S.; Leifer, K.; Hilborn, J.; Ossipov, D., Direct "Click" Synthesis of Hybrid Bisphosphonate-Hyaluronic Acid Hydrogel in Aqueous Solution for Biomineralization. *Chemistry of Materials* **2012**, 24, (9), 1690-1697.
31. Vasikaran, S. D., Bisphosphonates: an overview with special reference to alendronate. *Annals of Clinical Biochemistry* **2001**, 38, 608-623.
32. Heymann, D.; Ory, B.; Gouin, F.; Green, J. R.; Rédini, F., Bisphosphonates: new therapeutic agents for the treatment of bone tumors. *Trends in Molecular Medicine* **2004**, 10, (7), 337-343.
33. Martinez-Sanz, E.; Ossipov, D. A.; Hilborn, J.; Larsson, S.; Jonsson, K. B.; Varghese, O. P., Bone reservoir: Injectable hyaluronic acid hydrogel for minimal invasive bone augmentation. *Journal of Controlled Release* **2011**, 152, (2), 232-240.
34. Hench, L. L.; Polak, J. M., Third-Generation Biomedical Materials. *Science* **2002**, 295, (5557), 1014-1017.

35. Pitt, W. G.; Morris, R. N.; Mason, M. L.; Hall, M. W.; Luo, Y.; Prestwich, G. D., Attachment of hyaluronan to metallic surfaces. *Journal of Biomedical Materials Research Part A* **2004**, 68A, (1), 95-106.
36. Seror, J.; Merkher, Y.; Kampf, N.; Collinson, L.; Day, A. J.; Maroudas, A.; Klein, J., Articular Cartilage Proteoglycans As Boundary Lubricants: Structure and Frictional Interaction of Surface-Attached Hyaluronan and Hyaluronan-Aggregan Complexes. *Biomacromolecules* **2011**, 12, (10), 3432-3443.
37. Praveen, S. S.; Hanumantha, R.; Belovich, J. M.; Davis, B. L., Novel hyaluronic acid coating for potential use in glucose sensor design. *Diabetes Technology and Therapeutics* **2003**, 5, (3), 393-9.
38. Thierry, B.; Winnik, F. M.; Merhi, Y.; Silver, J.; Tabrizian, M., Bioactive Coatings of Endovascular Stents Based on Polyelectrolyte Multilayers. *Biomacromolecules* **2003**, 4, (6), 1564-1571.
39. Verheye, S.; Markou, C.; Salame, M.; Wan, B.; King, S.; Robinson, K.; Chronos, N.; Hanson, S., Reduced thrombus formation by hyaluronic acid coating of endovascular devices. *Arteriosclerosis Thrombosis and Vascular Biology* **2000**, 20, (4), 1168-1172.
40. Russell, T. P., *X-ray and Neutron Reflectivity for the Investigation of Polymers*. North-Holland, 1990; Vol. 5.
41. Buhler, E.; Boué, F., Persistence length for a model semirigid polyelectrolyte as seen by small angle neutron scattering: a relevant variation of the lower bound with ionic strength. *The European Physical Journal E: Soft Matter and Biological Physics* **2003**, 10, (2), 89-92.
42. Albersdörfer, A.; Sackmann, E., Swelling behavior and viscoelasticity ultrathin grafted hyaluronic acid films. *European Physical Journal B* **1999**, 10, (4), 663-672.
43. Hayashi, K.; Tsutsumi, K.; Nakajima, F.; Norisuye, T.; Teramoto, A., Chain-stiffness and excluded-volume effects in solutions of sodium hyaluronate at high ionic strength. *Macromolecules* **1995**, 28, (11), 3824-3830.
44. Orme, C. A.; Giocondi, J. L., *Chapter 9: Model Systems for Formation and Dissolution of Calcium Phosphate Minerals*. Handbook of Biomineralization, Model Systems for Formation and Dissolution of Calcium Phosphate Minerals, Wiley-VCH Verlag, Weinheim: United States, 2006.
45. Marshall, W. J., *Clinical chemistry*. Mosby: London, 1995; p 320.
46. Garrett, J. E.; Tamir, H.; Kifor, O.; Simin, R. T.; Rogers, K. V.; Mithal, A.; Gagel, R. F.; Brown, E. M., Calcitonin-secreting cells of the thyroid express an extracellular calcium receptor gene. *Endocrinology* **1995**, 136, (11), 5202-5211.
47. Gabriel, D. A.; Carr, M. E., Calcium destabilizes and causes conformational changes in hyaluronic acid. *American Journal of the Medical Sciences* **1989**, 298, (1), 8-14.
48. Sicińska, W.; Lerner, L. E., A detailed H-1 and C-13 NMR study of a repeating disaccharide of hyaluronan: The effect of sodium and calcium ions. *Carbohydrate Research* **1996**, 286, 151-159.
49. Rinaudo, M., Polyelectrolyte properties of a plant and animal polysaccharide. *Structural Chemistry* **2009**, 20, (2), 277-289.
50. Schexnaider, P.; Schmidt, G., Nanocomposite polymer hydrogels. *Colloid & Polymer Science* **2009**, 287, (1), 1-11.
51. Theunissen, E.; Overbergh, N.; Reynaers, H.; Antoun, S.; Jérôme, R.; Mortensen, K., Silica reinforced triblock copolymer gels. *Polymer* **2004**, 45, (6), 1857-1865.

52. Barrère, F.; van Blitterswijk, C. A.; de Groot, K., Bone regeneration: molecular and cellular interactions with calcium phosphate ceramics. *International Journal of Nanomedicine* **2006**, 1, (3), 317-332.
53. Jarcho, M., Calcium-phosphate ceramics as hard tissue prosthetics. *Clinical Orthopaedics and Related Research* **1981**, (157), 259-278.
54. Vallet-Regí, M.; González-Calbet, J. M., Calcium phosphates as substitution of bone tissues. *Progress in Solid State Chemistry* **2004**, 32, (1-2), 1-31.
55. Hu, Q.; Tan, Z.; Liu, Y.; Tao, J.; Cai, Y.; Zhang, M.; Pan, H.; Xu, X.; Tang, R., Effect of crystallinity of calcium phosphate nanoparticles on adhesion, proliferation, and differentiation of bone marrow mesenchymal stem cells. *Journal of Materials Chemistry* **2007**, 17, 4690-4698.
56. Lück, M.; Paulke, B. R.; Schröder, W.; Blunk, T.; Müller, R. H., Analysis of plasma protein adsorption on polymeric nanoparticles with different surface characteristics. *Journal of Biomedical Materials Research* **1998**, 39, (3), 478-485.
57. Owens, D. E.; Peppas, N. A., Opsonization, biodistribution, and pharmacokinetics of polymeric nanoparticles. *International Journal of Pharmaceutics* **2006**, 307, (1), 93-102.
58. Storm, G.; Belliot, S. O.; Daemen, T.; Lasic, D. D., Surface modification of nanoparticles to oppose uptake by the mononuclear phagocyte system. *Advanced Drug Delivery Reviews* **1995**, 17, (1), 31-48.
59. Moghimi, S. M.; Pavey, K. D.; Hunter, A. C., Real-time evidence of surface modification at polystyrene lattices by poloxamine 908 in the presence of serum: in vivo conversion of macrophage-prone nanoparticles to stealth entities by poloxamine 908. *FEBS Letters* **2003**, 547, (1-3), 177-182.
60. Blunk, T.; Hochstrasser, D. F.; Sanchez, J.-C.; Müller, B. W.; Müller, R. H., Colloidal carriers for intravenous drug targeting: Plasma protein adsorption patterns on surface-modified latex particles evaluated by two-dimensional polyacrylamide gel electrophoresis. *Electrophoresis* **1993**, 14, (1), 1382-1387.
61. García, A. J.; Ducheyne, P.; Boettiger, D., Cell adhesion strength increases linearly with adsorbed fibronectin surface density. *Tissue Engineering* **1997**, 3, (2), 197-206.
62. Park, J. W.; Lee, S. G.; Choi, B. J.; Suh, J. Y., Effects of a cell adhesion molecule coating on the blasted surface of titanium implants on bone healing in the rabbit femur. *International Journal of Oral & Maxillofacial Implants* **2007**, 22, (4), 533-541.
63. Reyes, C. D.; Petrie, T. A.; Burns, K. L.; Schwartz, Z.; García, A. J., Biomolecular surface coating to enhance orthopaedic tissue healing and integration. *Biomaterials* **2007**, 28, (21), 3228-35.
64. Kowalczyńska, H. M.; Nowak-Wyrzykowska, M.; Szczepankiewicz, A. A.; Dobkowski, J.; Dyda, M.; Kamiński, J.; Kołos, R., Albumin adsorption on unmodified and sulfonated polystyrene surfaces, in relation to cell-substratum adhesion. *Colloids and Surfaces B: Biointerfaces* **2011**, 84, (2), 536-544.
65. Norde, W., Surface-tethered polymers to influence protein adsorption and microbial adhesion. *Zeitschrift Für Physikalische Chemie-International Journal of Research in Physical Chemistry & Chemical Physics* **2007**, 221, (1), 47-63.
66. Fanali, G.; di Masi, A.; Trezza, V.; Marino, M.; Fasano, M.; Ascenzi, P., Human serum albumin: From bench to bedside. *Molecular Aspects of Medicine* **2012**, 33, (3), 209-290.

67. Carter, D. C.; Ho, J. X., Structure of serum-albumin. *Advances in Protein Chemistry* **1994**, 45, 153-203.
68. Galantini, L.; Leggio, C.; Pavel, N. V., Human Serum Albumin Unfolding: A Small-Angle X-ray Scattering and Light Scattering Study. *The Journal of Physical Chemistry B* **2008**, 112, (48), 15460-15469.
69. Brown, M. B.; Jones, S. A., Hyaluronic acid: a unique topical vehicle for the localized delivery of drugs to the skin. *Journal of the European Academy of Dermatology and Venereology* **2005**, 19, (3), 308-318.
70. Oates, K. M. N.; Krause, W. E.; Jones, R. L.; Colby, R. H., Rheopexy of synovial fluid and protein aggregation. *Journal of the Royal Society Interface* **2006**, 3, (6), 167-174.
71. Fraser, J. R. E.; Foo, W. K.; Maritz, J. S., Viscous interactions of hyaluronic acid with some proteins and neutral saccharides. *Annals of the Rheumatic Diseases* **1972**, 31, (6), 513-520.
72. Sugio, S.; Kashima, A.; Mochizuki, S.; Noda, M.; Kobayashi, K., Crystal structure of human serum albumin at 2.5 angstrom resolution. *Protein Engineering* **1999**, 12, (6), 439-446.
73. Scheufler, C.; Sebald, W.; Hülsmeier, M., Crystal structure of human bone morphogenetic protein-2 at 2.7 Å resolution. *Journal of Molecular Biology* **1999**, 287, (1), 103-115.
74. RCSB Protein Data Bank, www.rcsb.org/pdb/.
75. Wozney, J. M., Overview of bone morphogenetic proteins. *Spine* **2002**, 27, (16), S2-S8.
76. Liu, Y.; Huse, R. O.; de Groot, K.; Buser, D.; Hunziker, E. B., Delivery mode and efficacy of BMP-2 in association with implants. *Journal of Dental Research* **2007**, 86, (1), 84-89.
77. Hunziker, E. B.; Enggist, L.; Kueffer, A.; Buser, D.; Liu, Y., Osseointegration: The slow delivery of BMP-2 enhances osteoinductivity. *Bone* **2012**, 51, (1), 98-106.
78. Zara, J. N.; Siu, R. K.; Zhang, X.; Shen, J.; Ngo, R.; Lee, M.; Li, W.; Chiang, M.; Chung, J.; Kwak, J.; Wu, B. M.; Ting, K.; Soo, C., High Doses of Bone Morphogenetic Protein 2 Induce Structurally Abnormal Bone and Inflammation In Vivo. *Tissue Engineering Part A* **2011**, 17, (9-10), 1389-1399.
79. Seeherman, H.; Wozney, J.; Li, R., Bone morphogenetic protein delivery systems. *Spine* **2002**, 27, (16), 16-23.
80. Navarro, M.; Michiardi, A.; Castano, O.; Planell, J. A., Biomaterials in orthopaedics. *Journal of the Royal Society Interface* **2008**, 5, (27), 1137-1158.
81. Ossipov, D. A.; Piskounova, S.; Varghese, O. P.; Hilborn, J. n., Functionalization of Hyaluronic Acid with Chemoselective Groups via a Disulfide-Based Protection Strategy for In Situ Formation of Mechanically Stable Hydrogels. *Biomacromolecules* **2010**, 11, (9), 2247-2254.
82. Helling, M. S.; Kapaklis, V.; Rennie, A. R.; Hughes, A. V.; Porcar, L., Crystalline order of polymer nanoparticles over large areas at solid/liquid interfaces. *Applied Physics Letters* **2012**, 100, (22), 4.
83. Bendedouch, D.; Chen, S. H., Structure and interparticle interactions of bovine serum albumin in solution studied by small-angle neutron scattering. *Journal of Physical Chemistry* **1983**, 87, (9), 1473-1477.

84. Knox, P.; Levick, J. R.; McDonald, J. N., Synovial fluid - Its mass, macromolecular content and pressure in major limb joints of the rabbit. *Quarterly Journal of Experimental Physiology and Cognate Medical Sciences* **1988**, 73, (1), 33-45.
85. Martinez-Sanz, E.; Varghese, O. P.; Kisiel, M.; Engstrand, T.; Reich, K. M.; Bohner, M.; Jonsson, K. B.; Kohler, T.; Muller, R.; Ossipov, D. A.; Hilborn, J., Minimally invasive mandibular bone augmentation using injectable hydrogels. *Journal of tissue engineering and regenerative medicine* **2012**, 6 Suppl 3, s15-23.
86. Kisiel, M.; Martino, M. M.; Ventura, M.; Hubbell, J. A.; Hilborn, J.; Ossipov, D. A., Improving the osteogenic potential of BMP-2 with hyaluronic acid hydrogel modified with integrin-specific fibronectin fragment. *Biomaterials* **2013**, 34, (3), 704-712.
87. Kisiel, M.; Ventura, M.; Oommen, O. P.; George, A.; Walboomers, X. F.; Hilborn, J.; Varghese, O. P., Critical assessment of rhBMP-2 mediated bone induction: An in vitro and in vivo evaluation. *Journal of Controlled Release* **2012**, 162, (3), 646-653.
88. Berts, I. Properties of ideal polymeric vitreous substitutes. Uppsala University, Uppsala, 2009.
89. Goodwin, J. W.; Hughes, R. W., *Rheology for Chemists, An Introduction*. 2 ed.; The royal Society of Chemistry: Cambridge, 2008.
90. Rubenstein, M.; Colby, R. H., *Polymer Physics*. In Oxford University Press: Wiltshire, 2003.
91. Zackrisson, M.; Stradner, A.; Schurtenberger, P.; Bergenholtz, J., Small-angle neutron scattering on a core-shell colloidal system: A contrast-variation study. *Langmuir* **2005**, 21, (23), 10835-10845.
92. Dubruel, P.; Vanderleyden, E.; Bergada, M.; De Paepe, I.; Chen, H.; Kuypers, S.; Luyten, J.; Schrooten, J.; Van Hoorebeke, L.; Schacht, E., Comparative study of silanisation reactions for the biofunctionalisation of Ti-surfaces. *Surface Science* **2006**, 600, 2562-2571.
93. Rezania, A.; Johnson, R.; Lefkow, A. R.; Healy, K. E., Bioactivation of metal oxide surfaces. 1. Surface characterization and cell response. *Langmuir* **1999**, 15, (20), 6931-6939.
94. Kallury, K.; Macdonald, P.; Thompson, M., Effect of surface-water and base catalysis on the silanization of silica by (aminopropyl)alkoxysilanes studied by X-ray photoelectron-spectroscopy and C-13 cross-polarization/magic-angle-spinning nuclear-magnetic-resonance. *Langmuir* **1994**, 10, 492-499.
95. Wang, P.; Pan, G.; Hamilton, W. A.; Schaefer, D. W., Hydrothermal Degradation of Hydrophobic Organosilane Films Determined by Neutron Reflectometry. *Silanes and other coupling agents* **2009**, 5, 87.
96. Stile, R. A.; Barber, T. A.; Castner, D. G.; Healy, K. E., Sequential robust design methodology and X-ray photoelectron spectroscopy to analyze the grafting of hyaluronic acid to glass substrates. *Journal of Biomedical Materials Research* **2002**, 61, (3), 391-398.
97. Pasqui, D.; Atrei, A.; Barbucci, R., A novel strategy to obtain, a hyaluronan monolayer on solid substrates. *Biomacromolecules* **2007**, 8, (11), 3531-3539.
98. Sasaki, H.; Muramatsu, A.; Arakatsu, H.; Usui, S., ζ potential measurement by means of the plane interface technique. *Journal of Colloid and Interface Science* **1991**, 142, (1), 266-271.

99. Zhang, L.; Tian, C.; Waychunas, G. A.; Shen, Y. R., Structures and Charging of α -Alumina (0001)/Water Interfaces Studied by Sum-Frequency Vibrational Spectroscopy. *Journal of the American Chemical Society* **2008**, 130, (24), 7686-7694.
100. Kershner, R. J.; Bullard, J. W.; Cima, M. J., Zeta potential orientation dependence of sapphire substrates. *Langmuir* **2004**, 20, (10), 4101-4108.
101. Franks, G. V.; Meagher, L., The isoelectric points of sapphire crystals and alpha-alumina powder. *Colloids and Surfaces A: Physicochemical and Engineering Aspects* **2003**, 214, (1-3), 99-110.
102. Li, N.; Thomas, R. K.; Rennie, A. R., Effect of pH, surface charge and counter-ions on the adsorption of sodium dodecyl sulfate to the sapphire/solution interface. *Journal of Colloid and Interface Science* **2012**, 378, 152-158.
103. Hermanson, G. T., *Bioconjugate Techniques*. Academic Press: California, 1996.
104. Fagerholm, P.; Koul, S.; Trocmé, S., Corneal endothelial protection by heparin and sodium hyaluronate surface coating of PMMA intraocular lenses. *Acta Ophthalmologica* **1987**, 65, (S182), 110-114.
105. Grabarek, Z.; Gergely, J., Zero-Length Crosslinking Procedure with the Use of Active Esters. *Analytical Biochemistry* **1990**, 185, (1), 131-135.
106. Richert, L.; Boulmedais, F.; Lavalle, P.; Mutterer, J.; Ferreux, E.; Decher, G.; Schaaf, P.; Voegel, J. C.; Picart, C., Improvement of stability and cell adhesion properties of polyelectrolyte multilayer films by chemical cross-linking. *Biomacromolecules* **2004**, 5, (2), 284-294.
107. Pouyani, T.; Kuo, J. W.; Harbison, G. S.; Prestwich, G. D., Solid-state NMR of N-Acylureas Derived from the Reaction of Hyaluronic Acid with Isotopically-Labeled Carbodiimides. *Journal of the American Chemical Society* **1992**, 114, (15), 5972-5976.
108. Hellsing, M. S.; Rennie, A. R.; Porcar, L.; Englund, C. J., Scattering from Dilute and Lamellar Phase Solutions of Aerosol-OT Simultaneous Probe of Surface Structures and Bulk. *Progress in Colloid and Polymer Science* **2011**, 138, 139-142.
109. Azzam, R. M. A.; Bashara, N. M., *Ellipsometry and Polarized Light*. North Holland Publishing Company: 1977.
110. Powell, C. J.; Seah, M. P., Precision, accuracy, and uncertainty in quantitative surface analyses by Auger-electron spectroscopy and x-ray photoelectron spectroscopy. *Journal of Vacuum Science & Technology A: Vacuum, Surfaces, and Films* **1990**, 8, (2), 735-763.
111. Feiler, A. A.; Sahlholm, A.; Sandberg, T.; Caldwell, K. D., Adsorption and viscoelastic properties of fractionated mucin (BSM) and bovine serum albumin (BSA) studied with quartz crystal microbalance (QCM-D). *Journal of Colloid and Interface Science* **2007**, 315, (2), 475-481.
112. Höök, F.; Rodahl, M.; Brzezinski, P.; Kasemo, B., Energy Dissipation Kinetics for Protein and Antibody-Antigen Adsorption under Shear Oscillation on a Quartz Crystal Microbalance. *Langmuir* **1998**, 14, (4), 729-734.
113. Sauerbrey, G., Verwendung von Schwingquarzen zur Wägung dünner Schichten und zur Mikrowägung. *Zeitschrift Für Physik* **1959**, 155, (2), 206-222.
114. Höök, F. Development of a novel QCM technique for protein adsorption studies. Göteborg University, 2004.

115. Höök, F.; Voros, J.; Rodahl, M.; Kurrat, R.; Boni, P.; Ramsden, J. J.; Textor, M.; Spencer, N. D.; Tengvall, P.; Gold, J.; Kasemo, B., A comparative study of protein adsorption on titanium oxide surfaces using in situ ellipsometry, optical waveguide lightmode spectroscopy, and quartz crystal microbalance/dissipation. *Colloids and Surfaces B-Biointerfaces* **2002**, 24, (2), 155-170.
116. Martins, G. V.; Merino, E. G.; Mano, J. F.; Alves, N. M., Crosslink Effect and Albumin Adsorption onto Chitosan/Alginate Multilayered Systems: An in situ QCM-D Study. *Macromolecular Bioscience* **2010**, 10, (12), 1444-1455.
117. Dolatshahi-Pirouz, A.; Rechendorff, K.; Hovgaard, M. B.; Foss, M.; Chevallier, J.; Besenbacher, F., Bovine serum albumin adsorption on nano-rough platinum surfaces studied by QCM-D. *Colloids and Surfaces B-Biointerfaces* **2008**, 66, (1), 53-59.
118. Serro, A. P.; Degiampietro, K.; Colaco, R.; Saramago, B., Adsorption of albumin and sodium hyaluronate on UHMWPE: A QCM-D and AFM study. *Colloids and Surfaces B-Biointerfaces* **2010**, 78, (1), 1-7.
119. Malmström, J.; Agheli, H.; Kingshott, P.; Sutherland, D. S., Viscoelastic Modeling of highly hydrated laminin layers at homogeneous and nanostructured surfaces: Quantification of protein layer properties using QCM-D and SPR. *Langmuir* **2007**, 23, (19), 9760-9768.
120. Pynn, R., *Neutron Scattering - A Non-destructive Microscope for Seeing Inside Matter*. Springer: New York, 2009.
121. Lopez-Rubio, A.; Gilbert, E. P., Neutron scattering: a natural tool for food science and technology research. *Trends in Food Science & Technology* **2009**, 20, (11-12), 576-586.
122. Rauch, H.; Waschkowski, W., *Neutron properties*. Old City Publishing: Philadelphia, 2003.
123. Harroun, T. A.; Wignall, G. D.; Katsaras, J., *Neutron Scattering for Biology*. Springer Verlag: Berlin, 2006.
124. Sears, V. F., Neutron scattering lengths and cross sections. *Neutron News* **1992**, 3, (3), 26-37.
125. Munter, A. <http://www.ncnr.nist.gov/resources/sldcalc.html>.
126. Zaccai, G., Neutrons in biology in the post genome sequencing era. *Applied Physics A-Materials Science & Processing* **2002**, 74, 6-10.
127. Cubitt, R.; Fragneto, G., Neutron Reflection: Principles and Examples of Applications. In *Scattering in Microscopic Physics and Chemical Physics*, Pike, E. R.; Sabatier, P. C., Eds. Academic Press: London, 2002; pp 1198-1208.
128. Hammouda, B., Probing Nanoscale Structures – The SANS Toolbox. In http://www.ncnr.nist.gov/staff/hammouda/the_SANS_toolbox.pdf.
129. Jacrot, B., The study of biological structures by neutron scattering from solution. *Reports on Progress in Physics* **1976**, 911-953.
130. Boué, F.; Cousin, F.; Gummel, J.; Oberdisse, J.; Carrot, G.; El Harrak, A., Small angle scattering from soft matter—application to complex mixed systems. *Comptes Rendus Physique* **2007**, 8, (7-8), 821-844.
131. Higgins, J.; Benoît, H., *Polymers and neutron scattering*. Clarendon Press: Oxford, 1994.
132. Jha, A. K.; Hule, R. A.; Jiao, T.; Teller, S. S.; Clifton, R. J.; Duncan, R. L.; Pochan, D. J.; Jia, X., Structural Analysis and Mechanical Characterization of Hyaluronic Acid-Based Doubly Cross-Linked Networks. *Macromolecules* **2009**, 42, (2), 537-546.

133. Gerelli, Y.; Di Bari, M. T.; Deriu, A.; Cantu, L.; Colombo, P.; Como, C.; Motta, S.; Sonvico, F.; May, R., Structure and organization of phospholipid/polysaccharide nanoparticles. *Journal of Physics-Condensed Matter* **2008**, 20, (10), 8.
134. Hellsing, M. S.; Rennie, A. R.; Heenan, R. K.; Rogers, S. E., Structure of a large colloidal crystal - controlling orientation and three-dimensional order. *Rsc Advances* **2012**, 2, (18), 7091-7098.
135. Guinier, A.; Fournet, G., *Small-Angle Scattering of X-rays*. Wiley: New York, 1955.
136. Windsor, C. G., An Introduction to Small-Angle Neutron Scattering. *Journal of Applied Crystallography* **1988**, 21, 582-588.
137. Ramsay, J. D. F., Surface and pore structure characterisation by neutron scattering techniques. *Advances in Colloid and Interface Science* **1998**, 76-77, (0), 13-37.
138. Lieutenant, K.; Lindner, P.; Gahler, R., A new design for the standard pinhole small-angle neutron scattering instrument D11. *Journal of Applied Crystallography* **2007**, 40, (6), 1056-1063.
139. D22 <http://www.ill.eu/instruments-support/instruments-groups/instruments/d22/>.
140. D33 <http://www.ill.eu/instruments-support/instruments-groups/instruments/d33/>.
141. Ghosh, R. E.; Egelhaaf, S. U.; Rennie, A. R., *A Computing Guide for Small-Angle Scattering Experiments*. Institut Laue-Langevin Internal Publication ILL06GH05T: Grenoble, 2006.
142. Dewhurst, C. <http://www.ill.eu/instruments-support/instruments-groups/groups/lss/grasp/>.
143. Horkay, F.; Hecht, A. M.; Geissler, E., Similarities between polyelectrolyte gels and biopolymer solutions. *Journal of Polymer Science Part B-Polymer Physics* **2006**, 44, (24), 3679-3686.
144. Horkay, F.; Basser, P. J.; Hecht, A.-M.; Geissler, E., Structural investigations of a neutralized polyelectrolyte gel and an associating neutral hydrogel. *Polymer* **2005**, 46, (12), 4242-4247.
145. Geissler, E.; Horkay, F.; Hecht, A.-M., Scattering from network polydispersity in polymer gels. *Physical Review Letters* **1993**, 71, (4), 645-648.
146. Geissler, E.; Horkay, F.; Hecht, A.-M.; Rochas, C.; Lindner, P.; Bourgaux, C.; Couarraze, G., Investigation of PDMS gels and solutions by small angle scattering. *Polymer* **1997**, 38, (1), 15-20.
147. Kohlbrecher, J., *SASfit: A Program for Fitting Simple Structural Models to Small Angle Scattering Data*. Paul Scherrer Institut, Laboratory for Neutron Scattering: CH-5232, Villigen, Switzerland, 2008.
148. Cho, J.-H.; Alina, G.; Cortes Hernandez, R.; Butler, P.; Doucet, M.; Jackson, A.; Kienzle, P.; Kline, S.; Zhou, J. <http://danse.chem.utk.edu/sansview.html>.
149. Penfold, J.; Richardson, R. M.; Zarbakhsh, A.; Webster, J. R. P.; Bucknall, D. G.; Rennie, A. R.; Jones, R. A. L.; Cosgrove, T.; Thomas, R. K.; Higgins, J. S.; Fletcher, P. D. I.; Dickinson, E.; Roser, S. J.; McLure, I. A.; Hillman, A. R.; Richards, R. W.; Staples, E. J.; Burgess, A. N.; Simister, E. A.; White, J. W., Recent advances in the study of chemical surfaces and interfaces by specular neutron reflection. *Journal of the Chemical Society-Faraday Transactions* **1997**, 93, (22), 3899-3917.

150. Penfold, J.; Thomas, R. K., The application of the specular reflection of neutrons to the study of surfaces and interfaces. *Journal of Physics-Condensed Matter* **1990**, 2, (6), 1369.
151. Lu, J. R.; Thomas, R. K., Neutron reflection from wet interfaces. *Journal of the Chemical Society-Faraday Transactions* **1998**, 94, (8), 995-1018.
152. Kilbey II, S. M.; Ankner, J. F., Neutron reflectivity as a tool to understand polyelectrolyte brushes. *Current Opinion in Colloid & Interface Science* **2012**, 17, (2), 83-89.
153. Su, T. J.; Lu, J. R.; Thomas, R. K.; Cui, Z. F., Effect of pH on the Adsorption of Bovine Serum Albumin at the Silica/Water Interface Studied by Neutron Reflection. *The Journal of Physical Chemistry B* **1999**, 103, (18), 3727-3736.
154. Wacklin, H. P., Neutron reflection from supported lipid membranes. *Current Opinion in Colloid & Interface Science* **2010**, 15, (6), 445-454.
155. Fragneto-Cusani, G., Neutron reflectivity at the solid/liquid interface: examples of applications in biophysics. *Journal of Physics-Condensed Matter* **2001**, 13, (21), 4973-4989.
156. Thomas, R. K., Neutron reflection from liquid interfaces. *Annual Review of Physical Chemistry* **2004**, 55, (1), 391-426.
157. Born, M.; Wolfe, E., *Principle of optics*. Pergamon Press: Oxford, 1989.
158. Heavens, O. S., *Optical Properties of Thin Solid Films*. Butterworths: London, 1955.
159. LAMP http://www.ill.eu/data_treat/lamp/the-lamp-book/.
160. Cubitt, R.; Fragneto, G., D17: the new reflectometer at the ILL. *Applied Physics A-Materials Science & Processing* **2002**, 74, 329-331.
161. Campbell, R. A.; Wacklin, H. P.; Sutton, I.; Cubitt, R.; Fragneto, G., FIGARO: The new horizontal neutron reflectometer at the ILL. *European Physical Journal Plus* **2011**, 126, (11), 22.
162. Rennie, A. R. http://material.fysik.uu.se/Group_members/adrian/refprog.htm.
163. Rennie, A. R. http://material.fysik.uu.se/Group_members/adrian/cprof.htm.
164. Jones, R. A. L.; Richards, R. W., *Polymers at Surfaces and Interfaces*. Cambridge University Press: 1999.
165. Hulsart-Billstrom, G.; Hu, Q.; Bergman, K.; Jonsson, K. B.; Aberg, J.; Tang, R.; Larsson, S.; Hilborn, J., Calcium phosphates compounds in conjunction with hydrogel as carrier for BMP-2: A study on ectopic bone formation in rats. *Acta Biomaterialia* **2011**, 7, (8), 3042-3049.
166. Van Vlierberghe, S.; Dubruel, P.; Schacht, E., Biopolymer-Based Hydrogels As Scaffolds for Tissue Engineering Applications: A Review. *Biomacromolecules* **2011**, 12, (5), 1387-1408.
167. Peppas, N. A.; Hilt, J. Z.; Khademhosseini, A.; Langer, R., Hydrogels in biology and medicine: From molecular principles to bionanotechnology. *Advanced Materials* **2006**, 18, (11), 1345-1360.
168. Boyce, M. C.; Arruda, E. M., Constitutive models of rubber elasticity: A review. *Rubber Chemistry and Technology* **2000**, 73, (3), 504-523.
169. Treloar, L. R. G., *The Physics of Rubber Elasticity*. Oxford University Press: Oxford, 1975.
170. Nam, K.; Watanabe, J.; Ishihara, K., Network structure of spontaneously forming physically cross-link hydrogel composed of two-water soluble phospholipid polymers. *Polymer* **2005**, 46, (13), 4704-4713.
171. Horkay, F.; Hecht, A.-M.; Grillo, I.; Basser, P. J.; Geissler, E., Experimental evidence for two thermodynamic length scales in neutralized polyacrylate gels. *The Journal of Chemical Physics* **2002**, 117, (20), 9103-9106.

172. D'Errico, G.; De Lellis, M.; Mangiapia, G.; Tedeschi, A.; Ortona, O.; Fusco, S.; Borzacchiello, A.; Ambrosio, L., Structural and Mechanical Properties of UV-Photo-Cross-Linked Poly(N-vinyl-2-pyrrolidone) Hydrogels. *Biomacromolecules* **2008**, 9, (1), 231-240.
173. Peppas, N. A.; Bures, P.; Leobandung, W.; Ichikawa, H., Hydrogels in pharmaceutical formulations. *European Journal of Pharmaceutics and Biopharmaceutics* **2000**, 50, (1), 27-46.
174. Shibayama, M., Small Angle Neutron Scattering on Gels. In *Soft Matter Characterization*, Borsali, R.; Pecora, R., Eds. Springer: New York, 2008.
175. Buhler, E.; Boué, F., Chain persistence length and structure in hyaluronan solutions: Ionic strength dependence for a model semirigid polyelectrolyte. *Macromolecules* **2004**, 37, (4), 1600-1610.
176. Piskounova, S.; Rojas, R.; Bergman, K.; Hilborn, J., The Effect of Mixing on the Mechanical Properties of Hyaluronan-Based Injectable Hydrogels. *Macromolecular Materials and Engineering* **2011**, 296, (10), 944-951.
177. Hulsart, S. G. Influence of Calcium Phosphate on Osteogenesis in Hydrogel with Bone Morphogenetic Protein-2. Uppsala University, Uppsala, 2010.
178. Ollerton, A.; Werner, L.; Fuller, S. R.; Kavoussi, S. C.; McIntyre, J. S.; Mamalis, N., Evaluation of a new single-piece 4% water content hydrophobic acrylic intraocular lens in the rabbit model. *Journal of Cataract and Refractive Surgery* **2012**, 38, (10), 1827-1832.
179. Schwarz, F.; Wieland, M.; Schwartz, Z.; Zhao, G.; Rupp, F.; Geis-Gerstorfer, J.; Schedle, A.; Broggini, N.; Bornstein, M. M.; Buser, D.; Ferguson, S. J.; Becker, J.; Boyan, B. D.; Cochran, D. L., Potential of chemically modified hydrophilic surface characteristics to support tissue integration of titanium dental implants. *Journal of Biomedical Materials Research Part B: Applied Biomaterials* **2009**, 88B, (2), 544-557.
180. Song, D.; Forciniti, D., Effects of Cosolvents and pH on Protein Adsorption on Polystyrene Latex: A Dynamic Light Scattering Study. *Journal of Colloid and Interface Science* **2000**, 221, (1), 25-37.
181. Ortega-Vinuesa, J. L.; Tengvall, P.; Lundström, I., Molecular packing of HSA, IgG, and fibrinogen adsorbed on silicon by AFM imaging. *Thin Solid Films* **1998**, 324, (1-2), 257-273.
182. Magdassi, S.; Kamyshny, A., *Surface Activity of Proteins: Chemical and Physicochemical Modifications*. Marcel Dekker, Inc.: New York, 1996.

Acta Universitatis Upsaliensis

*Digital Comprehensive Summaries of Uppsala Dissertations
from the Faculty of Science and Technology 1043*

Editor: The Dean of the Faculty of Science and Technology

A doctoral dissertation from the Faculty of Science and Technology, Uppsala University, is usually a summary of a number of papers. A few copies of the complete dissertation are kept at major Swedish research libraries, while the summary alone is distributed internationally through the series Digital Comprehensive Summaries of Uppsala Dissertations from the Faculty of Science and Technology.



ACTA
UNIVERSITATIS
UPSALIENSIS
UPPSALA
2013

Distribution: publications.uu.se
urn:nbn:se:uu:diva-198357